

### Vector-boson production in supersymmetric QCD

Alan Axelrod

Department of Physics, Florida State University, Tallahassee, Florida 32306

(Received 15 December 1986)

Production in hadronic collisions of ordinary and possible new heavy charged or neutral vector bosons decaying to final states containing an  $e^+$  or  $e^-$  is studied in supersymmetric QCD. Parton distributions are computed for a number of assumptions about scalar-quark and gluino masses. For foreseeable energies, the scalar-quark-anti-scalar-quark annihilation contribution is at most a few percent of the quark-antiquark annihilation contribution. However, increased vector-boson decay widths and faster evolution of quark distributions in the supersymmetric case decrease cross sections by a factor of as much as 2-3 relative to the ordinary case. Other, more detailed observables are only marginally affected.

#### I. INTRODUCTION

The supersymmetric extension of the standard  $SU(3) \times SU(2) \times U(1)$  model of the strong and electroweak interactions has received much attention as a proposal for new physics.<sup>1-5</sup> Its popularity is motivated by theoretical arguments and biases, since as of yet it has no direct experimental confirmation. Experiment has provided only lower bounds on the masses of the expected new particles.

Spin-0 scalar quarks and spin- $\frac{1}{2}$  gluinos are predicted to exist as strongly interacting supersymmetric partners for the standard quarks and gluons, respectively. Excluding the analysis of recent data from the CERN  $\bar{p}p$  collider, model-dependent lower bounds of  $\approx 20$  GeV for scalar-quark masses  $M_{\tilde{q}}$  and  $\sim$  few GeV for the gluino mass  $M_{\tilde{g}}$  can be set.<sup>2,3,5</sup> An analysis of the UA1 data on missing-transverse-energy events<sup>6</sup> concludes that  $M_{\tilde{q}} > 65-75$  GeV and  $M_{\tilde{g}} > 60-70$  GeV if the photino is the lightest super-

symmetric particle (LSP), or  $M_{\tilde{q}} \gtrsim 45-60$  GeV and either  $M_{\tilde{g}} \lesssim 5$  GeV or  $\gtrsim 40$  GeV in the event that the Higgs fermion is the LSP.<sup>7</sup> However, uncertainty is introduced into these  $\bar{p}p$  bounds by the complex and necessarily imprecise modeling of experimental conditions.<sup>7</sup> The  $\bar{p}p$  bounds may also be weakened considerably if one relaxes the assumptions of left-right and five-flavor scalar-quark degeneracy, allows for  $R$ -parity violation,<sup>8</sup> or admits the possibility that the gluino is stable or nearly so, e.g., if it is the LSP, in which case there would be little or no missing energy in the relevant supersymmetric decay chains.

In the standard Drell-Yan model<sup>9</sup> supplemented with QCD corrections in the usual way,<sup>10</sup> production of weakly interacting vector bosons in  $pp$  or  $\bar{p}p$  collisions proceeds at lowest order by the quark-antiquark annihilation diagram of Fig. 1(a).<sup>11</sup> In the diagram, it is assumed that the vector boson subsequently decays into an  $\bar{l}l$  lepton pair. The quark, antiquark, and gluon distributions in the proton or antiproton at the  $Q^2$  of interest are determined in the leading-logarithm approximation by the Altarelli-Parisi integro-differential evolution equations,<sup>12</sup> once input distributions have been specified at some  $Q_0^2 < Q^2$ . The evolution proceeds via typical splittings such as  $q \rightarrow qg$ ,  $g \rightarrow q\bar{q}$ , and  $g \rightarrow gg$  shown in Fig. 2.

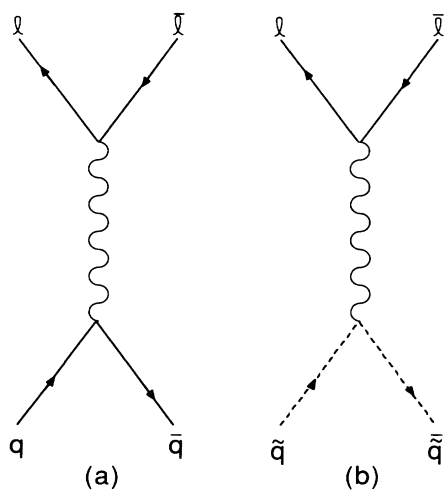


FIG. 1. Parton-model diagrams for  $p + p(\bar{p}) \rightarrow$  vector boson  $\rightarrow l + \bar{l}$ : (a) quark-antiquark annihilation; (b) scalar-quark-anti-scalar-quark annihilation.

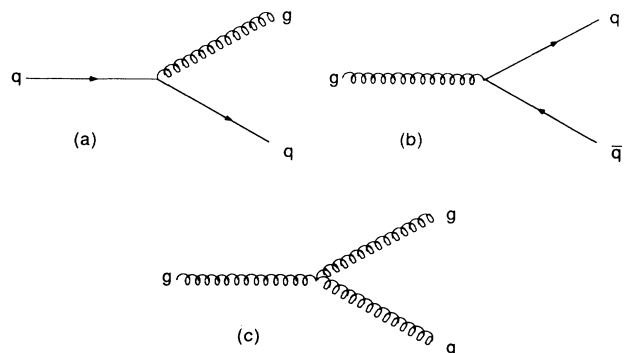


FIG. 2. Typical splitting diagrams for evolution of parton distributions in QCD: (a)  $q \rightarrow qg$ ; (b)  $g \rightarrow q\bar{q}$ ; (c)  $g \rightarrow gg$ .

However, in the supersymmetric theory considered here, the strongly interacting scalar quarks and/or gluinos participate in the evolution as well provided  $Q > \text{const} \times M_q$  and/or  $\text{const} \times M_g$  (Refs. 13–16). Typical supersymmetric splittings  $q \rightarrow \bar{q} \bar{g}$ ,  $g \rightarrow \bar{q} \bar{q}$ ,  $\bar{q} \rightarrow q \bar{g}$ , and  $\bar{g} \rightarrow g g$  are shown in Fig. 3. Thus, even if we start out with zero scalar-quark and gluino distributions at the initial  $Q_0$ , these distributions will be generated and become nonzero once the scalar-quark and/or gluino mass thresholds have been passed. This implies that scalar-quark–anti-scalar-quark annihilation, shown in Fig. 1(b), must be included for vector-boson production in addition to the usual quark–antiquark annihilation mechanism, since both are at zeroth order in  $\alpha_s$  in the standard QCD hard-scattering expansion.

A  $\bar{q}$ – $\bar{q}$  annihilation contribution can affect the angular distribution of the final-state leptons and reduce the magnitude of the associated forward-backward asymmetry. This is a consequence of angular momentum conservation as illustrated in Fig. 4. Since scalar quarks have spin 0, a left- or right-handed vector boson  $W_L^-$  or  $W_R^-$  must be produced with zero spin projection onto the  $\bar{q}$ – $\bar{q}$  axis of motion.  $W_L^-$  ( $W_R^-$ ) then decays into a left- (right-) handed electron and a right- (left-) handed antineutrino, so, if  $\theta$  is defined as the angle between the  $e^-$  and  $\bar{q}$  directions of motion in the  $W$  rest frame,  $\theta=0$  or  $\pi$  will violate angular momentum conservation. When  $\theta=\pi/2$ , the spin-0 projection component of the  $e^-$ – $\bar{q}$  system is maximized. Also, there is an obvious forward-backward  $\theta \leftrightarrow \pi - \theta$  symmetry. Not surprisingly, then, the angular distribution turns out to be proportional to  $\sin^2 \theta$ . On the other hand,  $q$ – $\bar{q}$  annihilations with  $V \pm A$  interactions can produce vector bosons with only  $\pm 1$  spin projections, which decay into leptons with asymmetric  $(1 \pm \cos \theta)^2$  distributions only; this is easily understood using similar angular momentum conservation arguments.<sup>17</sup> Also, because of the tendency of the scalar-quark-produced vector bosons to emit leptons at right angles to the beam direction in their rest frames, the shape of the lepton transverse-momentum distribution could be affected by the presence of initial scalar quarks.

As we shall see, however, the direct effect of  $\bar{q}$ – $\bar{q}$  annihilation will turn out to be small and unimportant com-

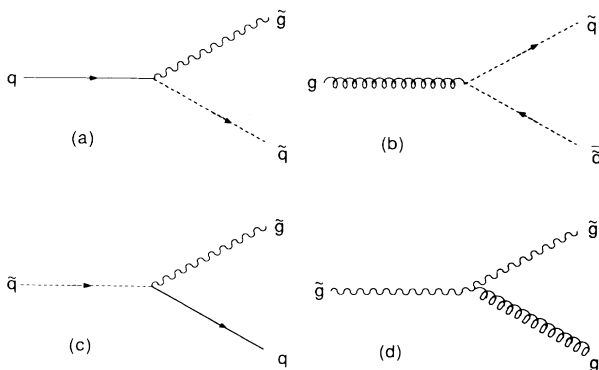


FIG. 3. Typical additional splitting diagrams occurring in supersymmetric QCD for evolution of parton distributions: (a)  $q \rightarrow \bar{q} \bar{g}$ ; (b)  $g \rightarrow \bar{q} \bar{q}$ ; (c)  $\bar{q} \rightarrow q \bar{g}$ ; (d)  $\bar{g} \rightarrow g \bar{g}$ .

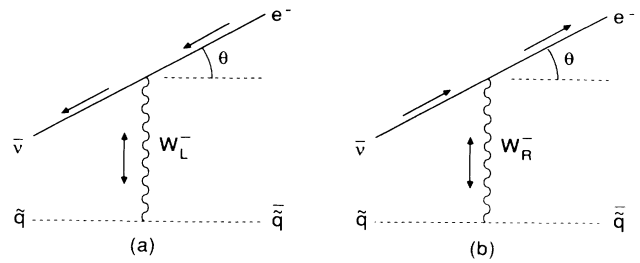


FIG. 4. Diagrams illustrating the effect of angular momentum conservation on the electron angular distribution in scalar-quark–anti-scalar-quark annihilation. The arrows denote spin direction. (a)  $W_L^-$  production; (b)  $W_R^-$  production.

pared to two other “indirect” effects of supersymmetry. First, the availability of supersymmetric decay final states for the vector bosons results in an increase in their total decay widths. This reduces the cross section for producing the leptonic final states studied in this paper by reducing the vector-boson branching ratios to these states. Second, the ordinary  $q$ – $\bar{q}$  annihilation contribution is altered since quark distributions lose momentum and evolve more rapidly when scalar quarks and gluinos are present. A greater depletion of quarks at relatively large  $x$  values can be expected to reduce cross sections for the production of heavy vector bosons.

As  $Q$  for the supersymmetric-QCD (SQCD) parton evolution is normally set equal to the mass of the produced vector boson, it is necessary to determine which vector bosons we want to consider here. The intermediate vector bosons  $W$  and  $Z$  of the standard model have been discovered at the CERN  $\bar{p}p$  collider<sup>18</sup> and have masses of  $\sim 100$  GeV. With the lower bounds on scalar-quark and gluino masses given above, large supersymmetric effects on vector-boson production should not be expected at this energy scale. However, it has been widely conjectured that new vector bosons with masses somewhat larger or much larger than 100 GeV may exist. These include right-handed  $W$ 's and new  $Z$ 's occurring in left-right gauge models,<sup>19</sup> new  $Z$ 's associated with extra U(1) factors appearing in breakings of SO(10) and  $E_6$  grand unified theories,<sup>20</sup> and extra vector bosons appearing in extended technicolor,<sup>21</sup> horizontal,<sup>22</sup> and composite<sup>23</sup> models. In particular, extra  $Z$ 's in  $E_6$  have recently been the subject of intensive phenomenological study<sup>24,25</sup> due to their appearance in the low-energy limit of the currently popular superstrings.<sup>26</sup> Lower mass bounds on new  $W$ 's and  $Z$ 's are generally surprisingly weak and  $\sim 100$ – $300$  GeV; a notable exception is a controversial and model-dependent lower bound on the  $W_R$  mass of 1.6 TeV from the  $K_L$ – $K_S$  mass difference.<sup>19</sup> On the other hand, a future high-energy hadronic collider such as the proposed Superconducting Super Collider (SSC) may be capable of discovering new vector bosons with masses  $\leq 10$  TeV.<sup>4,27</sup>

Therefore, in this work we investigate the potentially sizable effects of supersymmetry on the hadronic production cross sections of new  $W$ 's and  $Z$ 's with masses be-

tween 300 GeV and 10 TeV, as well as check for any possible effects on the production of the ordinary  $W$  and  $Z$ . Consideration is given to any effects on the lepton  $p_T$  distributions which are important for identifying new  $W$ 's and  $Z$ 's (Ref. 28) as well as old,<sup>29</sup> and on the forward-backward asymmetries which are thought to be useful for determining the new vector bosons' couplings.<sup>25,27,30</sup> This study will enable us to gauge how seriously the conclusions of earlier works would be affected by the plausible inclusion of supersymmetry into hadronic vector-boson production, which previously was neglected even in the superstring case where supersymmetry is manifest. For example, if a significant scalar-quark distribution were generated, it could be more difficult to determine vector-boson couplings by measuring forward-backward asymmetries.

The rest of this paper is organized as follows. In Sec. II the evolution of supersymmetric parton distributions is described. The Drell-Yan cross section formulas modified to include scalar-quark–anti-scalar-quark annihilation are given in Sec. III. The values chosen for various parameters are described in Sec. IV. We present our results in Sec. V for parton distributions, cross sections, angular distributions, asymmetries, and transverse-momentum distributions. Conclusions are in Sec. VI. The details of the integration of evolution equations are in Appendix A, while Appendix B contains a suggestion for analyzing lepton angular distributions.

## II. SUPERSYMMETRIC PARTON EVOLUTION

A computer program was developed that starts with ordinary parton distributions fit to experiment at some  $Q_0$ , evolves these upward in energy through various quark, scalar-quark, and/or gluino mass thresholds, and outputs the resulting parton distributions evaluated at some  $Q$ . As our main interest is to study sensitivity with respect to assumptions for scalar-quark and gluino masses, we fix the starting distributions to be the Duke and Owens set 1 “soft-gluon” fit at  $Q_0=2$  GeV; this has  $\Lambda=0.2$  GeV and an SU(3)-symmetric sea.<sup>31</sup> Conclusions are not expected to be sensitive to the choice of starting distributions, although it is worth pointing out that such a small value for  $\Lambda$  is also favored by Eichten, Hinchliffe, Lane, and Quigg (EHLQ) (0.20 GeV and 0.29 GeV for their set 1 and set 2 parton distributions, respectively).<sup>4</sup>

For evolution through mass thresholds, the standard “ $\Theta$ -function” approximation<sup>15,32</sup> of the effective-field-theory approach<sup>33</sup> is used. That is, heavy-particle distribution functions are assumed to be decoupled and zero for  $Q < nM_h$  but are coupled into the evolution and become nonzero for  $Q > nM_h$ , where  $M_h$  is the heavy-particle mass and  $n$  is a number  $\sim 1$ . Effectively, the assumption is that  $M_h \approx \infty$  for  $Q < nM_h$ , but  $M_h \approx 0$  for  $Q > nM_h$ . We choose  $n=2$ . The parton distributions are evaluated at the scale of the vector-boson mass  $M_B$ , which is the standard choice (e.g., see Ref. 4). It should be recognized that this leading-logarithm approximation is fairly crude for the large size of colored-particle masses that we will be considering, and may somewhat overesti-

mate the scalar-quark–anti-scalar-quark annihilation contribution.<sup>34</sup>

In order to reduce the set of possible evolutions to a representative sample of manageable size, some assumptions for colored-particle masses are required. Following Duke and Owens,  $Q_0=2$  GeV is taken to be the charm threshold;<sup>31</sup> we fix the bottom-quark mass  $M_b=5$  GeV and the top-quark mass  $M_t=50$  GeV, where the latter is at the upper end of the range suggested by UA1 data.<sup>35</sup> There are left-handed and right-handed scalar quarks corresponding to the two helicity components of each of the 6 quark flavors, for a total of 12 scalar quarks in all. For simplicity, we assume the maximum scalar-quark mass degeneracy compatible with all scalar quark flavors being at least as heavy as their quark partners. The latter requirement avoids a needless complication in the Altarelli-Parisi equations. In practice, this means that we assume 12-fold scalar-quark degeneracy, except that 10-fold degeneracy and  $M_{i_L}=M_{i_R}=M_i$  is assumed whenever the 10 scalar-quark masses are taken  $< M_t$ . These scalar-quark mass assumptions can be considered to approximate a less degenerate case. The gluino mass  $M_{\tilde{g}}$  is allowed to vary subject to  $M_{\tilde{g}} \geq M_b$ .

With these constraints in mind, a parton evolution subroutine was developed for each of the following nine possible cases, denoted for each case by the particles that are considered massless and thus participate in the evolution: (i) 4 quarks + gluon; (ii) 5 quarks + gluon; (iii) 6 quarks + gluon; (iv) 5 quarks + gluon + gluino; (v) 6 quarks + gluon + gluino; (vi) 5 quarks + gluon + 10 scalar quarks; (vii) 6 quarks + gluon + 12 scalar quarks; (viii) 5 quarks + gluon + gluino + 10 scalar quarks; (ix) 6 quarks + gluon + gluino + 12 scalar quarks.

The most general set of evolution equations, which is appropriate for cases (viii) and (ix), can be written as

$$\frac{dq_i(x,s)}{ds} = a_f [P_{qq} \otimes q_i + P_{qg} \otimes g + P_{q\tilde{g}} \otimes \tilde{g} + P_{q\tilde{q}} \otimes (\tilde{q}_{Li} + \tilde{q}_{Ri})], \quad (2.1)$$

$$\frac{dg(x,s)}{ds} = a_f (P_{gq} \otimes \Sigma + P_{gg} \otimes g + P_{g\tilde{g}} \otimes \tilde{g} + P_{g\tilde{q}} \otimes \tilde{\Sigma}), \quad (2.2)$$

$$\frac{d\tilde{g}(x,s)}{ds} = a_f (P_{\tilde{g}q} \otimes \Sigma + P_{\tilde{g}g} \otimes g + P_{\tilde{g}\tilde{g}} \otimes \tilde{g} + P_{\tilde{g}\tilde{q}} \otimes \tilde{\Sigma}), \quad (2.3)$$

$$\frac{d\tilde{q}_{Li}(x,s)}{ds} = a_f (P_{\tilde{q}q} \otimes q_i + P_{\tilde{q}g} \otimes g + P_{\tilde{q}\tilde{g}} \otimes \tilde{g} + P_{\tilde{q}\tilde{q}} \otimes \tilde{q}_{Li}), \quad (2.4)$$

and an equation identical to Eq. (2.4) except that  $L \rightarrow R$ . Here,  $q$ ,  $g$ ,  $\tilde{g}$ , and  $\tilde{q}$  are the quark, gluon, gluino, and scalar-quark distribution functions, respectively;  $i$  labels one of the  $N_f$  flavors and particle/antiparticle; the singlet-quark distribution is

$$\Sigma(x,s) = \sum_{i=1}^{2N_f} q_i(x,s) \quad (2.5)$$

and the singlet-scalar-quark distribution is

$$\bar{\Sigma}(x,s) = \sum_{i=1}^{2N_f} [\bar{q}_{Li}(x,s) + \bar{q}_{Ri}(x,s)] ; \quad (2.6)$$

$P_{ij}$  are the Altarelli-Parisi splitting kernels, and

$$A \otimes B = \int_x^1 \frac{dy}{y} A(y) B \left[ \frac{x}{y}, s \right]. \quad (2.7)$$

The variable controlling the evolution is

$$s = \ln[\ln(Q^2/\Lambda_f^2)/\ln(Q_0^2/\Lambda_f^2)], \quad (2.8)$$

where here  $Q_0$  defines the lower boundary of the evolution region of interest and  $\Lambda_f$  is the (S)QCD scale parameter appropriate to this evolution region, with the strong coupling constant given by

$$\frac{\alpha_s(Q^2)}{2\pi} = \frac{a_f}{\ln(Q^2/\Lambda_f^2)}. \quad (2.9)$$

For evolution cases (i)–(vii) above, the obviously irrelevant equations among Eqs. (2.1)–(2.4) are omitted, as are the irrelevant terms in the remaining equations.

$\Lambda_f$  in any evolution region is determined from  $\Lambda_i$  in the previous region by requiring  $\alpha_s$  to be continuous across the mass threshold, a common requirement in the literature.<sup>4,34,36,37</sup> This matching condition implies that

$$\Lambda_f = \Lambda_i (\Lambda_i/Q_0)^{(a_f/a_i-1)}. \quad (2.10)$$

The splitting functions  $P_{ij}$  can be found in the literature.<sup>4,12–16,38,39</sup> It should be noted that the diagonal  $P_{ii}$ 's have coefficients of their  $\delta(1-x)$  terms that vary according to what set of particles are coupled to the evolution, but which are easily determined by requiring the baryon-number and momentum conservation sum rules to be satisfied.<sup>15</sup>

In each region, the evolution is “diagonalized” to as great an extent as possible by evolving a minimal set of nonsinglet and singlet distributions. Rather than tabulating all nine cases, we illustrate this strategy by considering the two extreme examples, cases (i) and (ix). In the 4 quarks + gluon case (i), valence up- and down-quark and nonsinglet charm-quark distributions are defined by

$$u_v(x,s) = u(x,s) - \bar{u}(x,s), \quad (2.11)$$

$$d_v(x,s) = d(x,s) - \bar{d}(x,s), \quad (2.12)$$

$$\Sigma_c(x,s) = \Sigma(x,s) - 8c(x,s). \quad (2.13)$$

These evolve diagonally by

$$\frac{dQ(x,s)}{ds} = a_f P_{qq} \otimes Q, \quad (2.14)$$

where  $Q$  is either  $u_v$ ,  $d_v$ , or  $\Sigma_c$ .  $\Sigma$  and  $g$  evolve by a  $2 \times 2$  matrix coupled singlet equation:

$$\frac{d}{ds} \begin{bmatrix} \Sigma(x,s) \\ g(x,s) \end{bmatrix} = a_f \begin{bmatrix} P_{qq} & 8P_{qg} \\ P_{gq} & P_{gg} \end{bmatrix} \otimes \begin{bmatrix} \Sigma \\ g \end{bmatrix}. \quad (2.15)$$

In this and similar equations,  $\otimes$  includes matrix multiplication as well as the convolution of Eq. (2.7). Using the

assumed symmetries, any other particle or antiparticle distribution can then be written as a function of these five. In the 6 quarks + gluon + gluino + 12 scalar quarks case (ix), however, 14 independent distributions are required. Ten of these are valence or nonsinglet (the arguments  $x, s$  are omitted here):

$$u_v = u - \bar{u}, \quad (2.16)$$

$$\bar{u}_v = \bar{u}_L + \bar{u}_R - \bar{u}_L - \bar{u}_R, \quad (2.17)$$

$$d_v = d - \bar{d}, \quad (2.18)$$

$$\bar{d}_v = \bar{d}_L + \bar{d}_R - \bar{d}_L - \bar{d}_R, \quad (2.19)$$

$$\Sigma_c = \Sigma - 12c, \quad (2.20)$$

$$\bar{\Sigma}_c = \bar{\Sigma} - 12(\bar{c}_L + \bar{c}_R), \quad (2.21)$$

$$\Sigma_b = \Sigma - 12b, \quad (2.22)$$

$$\bar{\Sigma}_b = \bar{\Sigma} - 12(\bar{b}_L + \bar{b}_R), \quad (2.23)$$

$$\Sigma_t = \Sigma - 12t, \quad (2.24)$$

$$\bar{\Sigma}_t = \bar{\Sigma} - 12(\bar{t}_L + \bar{t}_R), \quad (2.25)$$

which evolve via five  $2 \times 2$  matrix equations,

$$\frac{d}{ds} \begin{bmatrix} Q(x,s) \\ \bar{Q}(x,s) \end{bmatrix} = a_f \begin{bmatrix} P_{qq} & P_{q\bar{q}} \\ 2P_{\bar{q}q} & P_{\bar{q}\bar{q}} \end{bmatrix} \otimes \begin{bmatrix} Q \\ \bar{Q} \end{bmatrix}, \quad (2.26)$$

where  $Q$  can be  $u_v$ ,  $d_v$ ,  $\Sigma_c$ ,  $\Sigma_b$ , or  $\Sigma_t$ . The remaining singlet distributions  $\Sigma$ ,  $g$ ,  $\bar{g}$ , and  $\bar{\Sigma}$  evolve in a  $4 \times 4$  coupled matrix equation:

$$\frac{d}{ds} \begin{bmatrix} \Sigma(x,s) \\ g(x,s) \\ \bar{g}(x,s) \\ \bar{\Sigma}(x,s) \end{bmatrix} = a_f \begin{bmatrix} P_{qq} & 12P_{qg} & 12P_{q\bar{g}} & P_{q\bar{q}} \\ P_{gq} & P_{gg} & P_{g\bar{g}} & P_{g\bar{q}} \\ P_{\bar{g}q} & P_{\bar{g}g} & P_{\bar{g}\bar{g}} & P_{\bar{g}\bar{q}} \\ 2P_{\bar{q}q} & 24P_{\bar{q}g} & 24P_{\bar{q}\bar{g}} & P_{\bar{q}\bar{q}} \end{bmatrix} \otimes \begin{bmatrix} \Sigma \\ g \\ \bar{g} \\ \bar{\Sigma} \end{bmatrix}. \quad (2.27)$$

Again, using the assumed degeneracies, any other particle or antiparticle distribution can be written in terms of these 14 “independent” ones. The other cases (ii)–(viii) interpolate in complexity between (i) and (ix) above. The matching conditions for the nonsinglet and singlet distributions at the boundaries between evolution regions are determined by the requirement that all individual particle and antiparticle distributions be continuous.<sup>32</sup>

In practice, in order to avoid singular behavior near  $x=0$ , all integro-differential evolution equations are written in terms of  $x^2$  times the parton distributions, rather than the parton distributions themselves. Then, beginning with the parton distributions at  $Q_0$ , the computer program numerically integrates the evolution equations in the first region, performs matching at the boundary with the second region, numerically integrates in the second region, etc., until  $Q$  is reached, at which point the parton distributions evaluated at  $Q$  are output. The numerical integration procedure used, accuracy, and checks are discussed in Appendix A.

### III. MODIFIED DRELL-YAN MODEL

We wish to study the process  $p + (p \text{ or } \bar{p}) \rightarrow B \rightarrow e^\pm + l$ , where  $B$  is some intermediate vector boson and  $l$  is a lepton. To this end, we consider the neutral-current Lagrangian

$$L_{\text{NC}} = gB_\mu \left[ \sum_j \bar{q}_j (a_j \gamma^\mu + b_j \gamma^\mu \gamma_5) q_j + i \sum_m \bar{a}_m (\bar{q}_m^* \vec{\partial}^\mu \bar{q}_m) + \bar{e} (c_e \gamma^\mu + d_e \gamma^\mu \gamma_5) e \right] \quad (3.1)$$

or the charged-current Lagrangian

$$L_{\text{CC}} = gB_\mu \left[ \sum_{jk} \bar{q}_j (a_{jk} \gamma^\mu + b_{jk} \gamma^\mu \gamma_5) q_k + i \sum_{mn} \bar{a}_{mn} (\bar{q}_m^* \vec{\partial}^\mu \bar{q}_n) + \bar{\nu} (c_{\nu e} \gamma^\mu + d_{\nu e} \gamma^\mu \gamma_5) e \right] + \text{H.c.} , \quad (3.2)$$

where  $q$  represents quarks and  $\bar{q}$  scalar quarks;  $a, b, \bar{a}, c,$  and  $d$  are real couplings;  $j, k$  label allowed quark flavors; and  $m, n$  label allowed scalar-quark flavors and  $L, R$ .  $\nu$  is considered in this section to be a Dirac neutrino, but since neutrino masses are neglected and later the charged  $B$  will be taken to be  $W_L$  or  $W_R$ , results will be the same for Majorana as for Dirac (Weyl) neutrinos.<sup>40</sup> The rest of the formulas in this section are valid for either  $L_{\text{NC}}$  or  $L_{\text{CC}}$  and the subscripts on the couplings will be dropped as the relevant ones are obvious in each case.

For (quark from hadron  $h_1$ ) + (antiquark from hadron  $h_2$ ) annihilation producing a measured  $e^-$ , the double-differential cross section in  $y$ , the rapidity of  $B$  in the  $h_1$ - $h_2$  center-of-mass frame, and  $\cos\theta$ , the cosine of the angle between the electron and  $h_1$  directions of motion in the  $B$  rest frame, is

$$\frac{d^2\sigma}{dy d \cos\theta} = \left[ \frac{g^4}{384\Gamma_B M_B} \right] \sum_{jk} x_1 x_2 f_{h_1}^j(x_1) f_{h_2}^k(x_2) \{ [(c+d)^2(a+b)^2 + (c-d)^2(a-b)^2](1+\cos\theta)^2 + [(c+d)^2(a-b)^2 + (c-d)^2(a+b)^2](1-\cos\theta)^2 \} , \quad (3.3)$$

where

$$x_1 = \frac{M_B}{\sqrt{s}} e^y , \quad (3.4)$$

$$x_2 = \frac{M_B}{\sqrt{s}} e^{-y} , \quad (3.5)$$

$M_B$  and  $\Gamma_B$  are the vector-boson mass and total decay width, respectively,  $s$  is the hadron-hadron center-of-mass invariant, and  $f_{h_1}^j$  ( $f_{h_2}^k$ ) is the distribution function for parton  $j$  ( $k$ ) in hadron  $h_1$  ( $h_2$ ). All particles besides  $B$  are treated as massless, and the pole approximation to the vector-boson propagator has been used. With the convention that  $\theta$  is always measured relative to  $h_1$ 's direction of motion, Eq. (3.3) is unchanged if the antiquark comes from  $h_1$  and a produced  $e^+$  is measured; however, for a quark from  $h_1$  and  $e^+$  measured, or for an antiquark from  $h_1$  and  $e^-$  measured, it is necessary to replace  $\cos\theta \rightarrow -\cos\theta$ .

With the same assumptions and conventions, the scalar-quark-anti-scalar-quark annihilation formula analogous to Eq. (3.3) is

$$\frac{d^2\sigma}{dy d \cos\theta} = \left[ \frac{g^4}{96\Gamma_B M_B} \right] \sum_{mn} x_1 x_2 f_{h_1}^m(x_1) f_{h_2}^n(x_2) [(c+d)^2 + (c-d)^2] \bar{a}^2 \sin^2\theta , \quad (3.6)$$

where Eqs. (3.4) and (3.5) still hold. Equation (3.6) is the same regardless of whether the scalar quark or the anti-scalar-quark is from  $h_1$  or whether an  $e^-$  or an  $e^+$  is measured. The factor of 4 difference between the coefficients in Eqs. (3.3) and (3.6) can be understood as due to initial quark and antiquark spin averaging whereas initial scalar quarks and anti-scalar-quarks are fixed to be  $L$  or  $R$ .

By convention,<sup>27</sup>  $h_1$  will always be taken to be a proton, whereby  $h_2$  will be a proton or antiproton as the case may be. After summing over all initial quark and scalar-quark contributions, integrations of  $d^2\sigma/dy d \cos\theta$  over  $\cos\theta$  and/or  $y$  give  $d\sigma/dy$ ,  $d\sigma/d \cos\theta$ , and  $\sigma$ . The rapidity is bounded by

$$-\ln[(\sqrt{s})/M_B] \leq y \leq \ln[(\sqrt{s})/M_B] , \quad (3.7)$$

and the  $y$  integrations are easily done numerically. The forward-backward asymmetry at fixed rapidity  $y$  is defined as

$$A_{\text{FB}}(y) = \left[ \left[ \int_0^1 - \int_{-1}^0 \right] d \cos\theta \frac{d^2\sigma}{dy d \cos\theta} \right] / \left[ \frac{d\sigma}{dy} \right] . \quad (3.8)$$

The total forward-backward asymmetry is defined similarly as

$$A_{\text{TFB}} = \left[ \left[ \int_0^1 - \int_{-1}^0 \right] d \cos \theta \frac{d \sigma}{d \cos \theta} \right] / \sigma . \quad (3.9)$$

Now consider the double-differential cross section in the measured  $e^\pm$  transverse momentum  $p_T$  and rapidity  $y_e$  in the  $h_1$ - $h_2$  center-of-mass frame. Restricting attention to rapidity  $y_e = 0$ , one finds for quark-antiquark annihilation that

$$\begin{aligned} \frac{d^2 \sigma}{dp_T dy_e} \Big|_{y_e=0} &= \left( \frac{g^4 p_T^3}{24\pi} \right) \sum_{jk} \sum_{\pm} \int d\hat{s} x_1 x_2 f_{h_1}^j(x_1) f_{h_2}^k(x_2) \frac{1}{\hat{s}^{5/2}} \frac{1}{(\hat{s} - 4p_T^2)^{1/2}} \frac{1}{(\hat{s} - M_B^2)^2 + \Gamma_B^2 M_B^2} \\ &\times \left[ [(c+d)^2(a+b)^2 + (c-d)^2(a-b)^2] u_{\pm}^2 \right. \\ &\quad \left. + [(c+d)^2(a-b)^2 + (c-d)^2(a+b)^2] \left[ \frac{\hat{s}}{u_{\pm}} \right]^2 \right], \end{aligned} \quad (3.10)$$

where

$$x_1 = \frac{\hat{s}}{u_{\pm} \sqrt{s}}, \quad (3.11)$$

$$x_2 = \frac{u_{\pm}}{\sqrt{s}}, \quad (3.12)$$

$$u_{\pm} = \frac{\hat{s}}{2p_T} [1 \pm (1 - 4p_T^2/\hat{s})^{1/2}], \quad (3.13)$$

and the integral over the quark-antiquark center-of-mass invariant  $\hat{s}$  is bounded by

$$4p_T^2 \leq \hat{s} \leq \frac{sp_T}{\sqrt{s} - p_T}. \quad (3.14)$$

Similarly to Eq. (3.3), Eq. (3.10) is strictly speaking valid only for a quark from  $h_1$  and  $e^-$  produced and measured, or an antiquark from  $h_1$  and  $e^+$  measured. For the other two combinations, it is necessary to interchange  $u_{\pm} \leftrightarrow \hat{s}/u_{\pm}$  in the expression inside the large square brackets.

Note that the smeared square-root singularity giving rise to the well-known Jacobian peak<sup>41</sup> at  $p_T = (\hat{s})^{1/2}/2 \approx M_B/2$  is manifest in this way of writing the  $p_T$  distribution. The full vector-boson propagator has been kept since, as is evident from the formula, the pole approximation is poor for  $p_T \gtrsim M_B/2$ .  $u_{\pm}$  correspond to the possibilities  $x_1 < x_2$  or  $x_1 > x_2$ .

The scalar-quark-anti-scalar-quark annihilation contribution analogous to Eq. (3.10) is

$$\begin{aligned} \frac{d^2 \sigma}{dp_T dy_e} \Big|_{y_e=0} &= \left( \frac{g^4 p_T^3}{6\pi} \right) \sum_{mn} \sum_{\pm} \int d\hat{s} x_1 x_2 f_{h_1}^m(x_1) f_{h_2}^n(x_2) \frac{1}{\hat{s}^{3/2}} \\ &\times \frac{1}{(\hat{s} - 4p_T^2)^{1/2}} \frac{1}{(\hat{s} - M_B^2)^2 + \Gamma_B^2 M_B^2} [(c+d)^2 + (c-d)^2] \bar{a}^2, \end{aligned} \quad (3.15)$$

where Eqs. (3.11)–(3.14) still hold. As with Eq. (3.6), Eq. (3.15) is the same regardless of which initial particle is from  $h_1$  or whether  $e^-$  or  $e^+$  is measured. The Jacobian peak is still apparent, but the functional dependence on  $p_T$  is different than in Eq. (3.10). Again, note the factor of 4 difference due to the spin averaging.

It should be emphasized that, aside from using  $Q^2$ -dependent parton distributions, Eqs. (3.3), (3.6), (3.10), and (3.15) use the simple massless parton model. In particular, effects of parton intrinsic transverse momentum and (S)QCD corrections such as gluon bremsstrahlung and  $K$  factors have been neglected.<sup>10,37,42</sup> The QCD  $K$  factor is  $\approx 1.3$  for ordinary  $W$  or  $Z$  production and is presumably closer to 1 for more massive vector bosons; it has also been argued that QCD effects on the lepton  $p_T$

distribution may become smaller for more massive vector bosons.<sup>28</sup> In any case, it is reasonable to expect that these neglected effects would change the quark and scalar-quark contributions, as well as change the quark contribution in the supersymmetric versus nonsupersymmetric cases, in roughly equal or sufficiently small manners so as not to affect conclusions about differences between the results in the supersymmetric and nonsupersymmetric cases.

#### IV. COUPLINGS AND PARAMETERS

The scalar-quark and gluino masses are subject to the experimental constraints discussed in the Introduction and to the simplicity requirements imposed in Sec. II, but up to this point are otherwise unrestricted. To check for

sensitivity of the results on mass assumptions, we consider six possible scenarios: (A) light gluino, heavy scalar quark:  $M_{\tilde{g}}=5$  GeV,  $M_{\tilde{q}}=100$  GeV; (B) heavy gluino, light scalar quark:  $M_{\tilde{g}}=100$  GeV,  $M_{\tilde{q}}=20$  GeV; (C) light gluino, light scalar quark:  $M_{\tilde{g}}=5$  GeV,  $M_{\tilde{q}}=20$  GeV; (D) heavy gluino, heavy scalar quark:  $M_{\tilde{g}}=100$  GeV,  $M_{\tilde{q}}=100$  GeV; (E) intermediate gluino and scalar quark:  $M_{\tilde{g}}=50$  GeV,  $M_{\tilde{q}}=50$  GeV; (F) ordinary nonsupersymmetric:  $M_{\tilde{g}}=M_{\tilde{q}}=\infty$ .

As described in Sec. II, if  $M_{\tilde{q}} < M_t = 50$  GeV, we set  $M_{\tilde{t}} = 50$  GeV. Scenarios (B) and (C), and also (A) and (E) if the photino is the LSP, are disfavored by the analysis of the UA1 data. However, as discussed in the Introduction, it is believed that there is sufficient uncertainty in that analysis to warrant consideration of all these scenarios to establish what effects could be expected from supersymmetric particles with such masses.

For the ordinary  $W$  and  $Z$  masses, we take the average of the UA1 (Ref. 43) and UA2 (Ref. 44) results:

$$M_W = 82.4 \text{ GeV} , \quad (4.1)$$

$$M_Z = 92.8 \text{ GeV} , \quad (4.2)$$

which by the usual tree-level relation (or all orders definition)

$$\sin^2 \theta_W = 1 - M_W^2 / M_Z^2 \quad (4.3)$$

gives

$$\sin^2 \theta_W = 0.212 , \quad (4.4)$$

which is also the average of the UA1 and UA2 values obtained using this formula.<sup>43,44</sup> By running the electromagnetic coupling constant up to  $M_W$ , the  $SU(2)_L$  coupling in the absence of supersymmetric particles is found to be

$$g(M_W) = \left[ \frac{4\pi\alpha_{EM}(M_W)}{\sin^2 \theta_W} \right]^{1/2} = 0.6807 . \quad (4.5)$$

In light-scalar-quark scenarios (B) and (C), this is changed to

$$g(M_W) = 0.6823 , \quad (4.6)$$

where any possible contribution of supersymmetric particles other than scalar quarks to the  $\beta$  function has been neglected. Cabibbo-Kobayashi-Maskawa mixing is neglected throughout this paper.

It is likely that new superheavy vector bosons will be associated with some new gauge group. For simplicity, we ignore theoretical bias and consider only superheavy copies<sup>4</sup> of the  $W$  and  $Z^0$  of the standard  $SU(2)_L \times U(1)$  model, with couplings fixed by Eqs. (4.4) and (4.6) and mixing between light and heavy vector bosons neglected.<sup>27</sup> All results of this paper for left-handed  $W$ 's will be the same for right-handed  $W$ 's. The superheavy masses are chosen to be

$$M_W, M_Z = 0.3, 1, 2, 5, \text{ or } 10 \text{ TeV} . \quad (4.7)$$

Even if it had been assumed that  $g(10 \text{ TeV})$  of the superheavy gauge group was equal to the renormalization-

group-evolved  $g(M_W)$ , using the formulas of Ref. 45 with 3 (super)generations the change from Eq. (4.6) would have been only  $-4\%$  for the nonsupersymmetric case or  $+1\%$  for the supersymmetric case, which is negligible.

For the decay widths of ordinary  $W$  and  $Z$  in the non-supersymmetric case, for three generations and taking into account phase-space suppression for decays involving top quarks, we obtain

$$\Gamma_W = 2.63 \text{ GeV} , \quad (4.8)$$

$$\Gamma_Z = 2.70 \text{ GeV} . \quad (4.9)$$

In the light-scalar-quark scenarios (B) and (C), channels are open for ordinary  $W$  and  $Z$  to decay into scalar quarks. Indeed, in a supersymmetric theory, every particle has a supersymmetric partner. For simplicity and to minimize the increase in the widths, it is assumed that scalar-lepton, gaugino, and Higgs-fermion decay channels are either kinematically forbidden or negligible; this is of course consistent with the experimental constraints.<sup>2,3,5</sup> Including the scalar-quark channels and taking phase-space suppressions into account, the supersymmetric decay widths of ordinary  $W$  and  $Z$  become

$$\Gamma_W = 3.20 \text{ GeV} , \quad (4.10)$$

$$\Gamma_Z = 3.40 \text{ GeV} . \quad (4.11)$$

Assuming three massless generations, the decay widths for superheavy  $W$  and  $Z$  in the nonsupersymmetric case are

$$\Gamma_W = \frac{g^2 M_W}{4\pi} , \quad (4.12)$$

$$\Gamma_Z = \frac{g^2 M_Z}{12\pi \cos^2 \theta_W} (3 - 6 \sin^2 \theta_W + 8 \sin^4 \theta_W) . \quad (4.13)$$

For the supersymmetric cases, assuming three complete massless supergenerations and neglecting gaugino, Higgs-fermion, and any other channels, the superheavy  $W$  and  $Z$  decay widths become

$$\Gamma_W = \frac{3g^2 M_W}{8\pi} , \quad (4.14)$$

$$\Gamma_Z = \frac{g^2 M_Z}{8\pi \cos^2 \theta_W} (3 - 6 \sin^2 \theta_W + 8 \sin^4 \theta_W) , \quad (4.15)$$

50% larger than in the nonsupersymmetric case. Branching ratios into electron final states can be computed for any case using

$$\Gamma(W \rightarrow e\nu) = \frac{g^2 M_W}{48\pi} , \quad (4.16)$$

$$\Gamma(Z \rightarrow e^+ e^-) = \frac{g^2 M_Z}{96\pi \cos^2 \theta_W} (1 - 4 \sin^2 \theta_W + 8 \sin^4 \theta_W) . \quad (4.17)$$

It is always implicitly assumed that a relatively pure sample of direct  $e^\pm$ 's from  $W, Z \rightarrow e^\pm + l$  can be isolated experimentally and studied. However, electrons can also be produced in other ways, e.g., as secondary products in

decay chains such as  $W \rightarrow \bar{e} \tilde{\nu} \rightarrow e \tilde{\gamma} \tilde{\nu}$  or  $Z \rightarrow \bar{e} \tilde{e} \rightarrow ee \tilde{\gamma} \tilde{\gamma}$ , or from decays of produced gauginos that may not differ greatly in mass from their associated gauge bosons.<sup>2</sup> Also, electrons from ordinary  $W$  and  $Z$  decays will present a background to those from superheavy-vector-boson decays.<sup>28</sup> Therefore, it is assumed that some combination of experimental cuts on electron momentum, missing momentum, or invariant mass can largely eliminate these extra electrons from the sample.

## V. RESULTS

Results for parton distributions, cross sections, angular distributions and asymmetries, and transverse momentum distributions are now discussed. The main focus will be on comparisons between the supersymmetric and nonsupersymmetric cases, since as noted earlier the nonsupersymmetric case has been adequately studied elsewhere.

### A. Parton distributions

With the introduction of scalar quarks and gluinos into the Altarelli-Parisi evolution equations, two main effects relevant to the subject of this paper are observed. First, scalar-quark distributions are generated, but very slowly. Second, the quark distributions evolve somewhat faster to smaller  $x$ .

As described in Appendix A, parton distributions are computed at fixed  $Q^2$  for a mesh in  $x$ , and interpolation in  $x$  is done using the method of cubic splines. Therefore, we do not have a parametrization of our distributions in a form suitable for publication. Instead, some illustrative results are shown in Figs. 5–9. It is emphasized that we have computed our own set of parton distributions in all cases, both supersymmetric and nonsupersymmetric.

In Fig. 5 we plot up-flavored distributions in the maximal scalar-quark-generating scenario considered in this paper: light-gluino, light-scalar-quark case (C) evaluated at  $Q = 10$  TeV. The up-scalar-quark distribution plotted

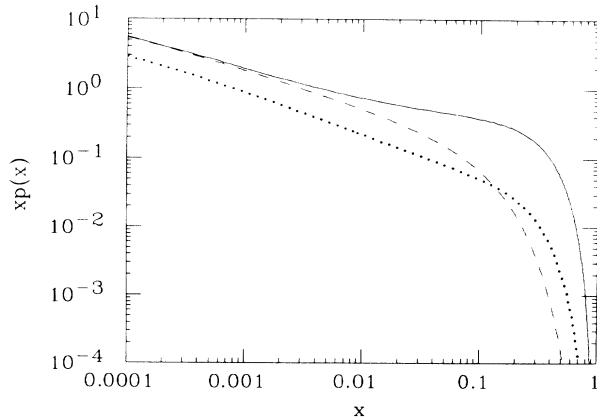


FIG. 5. Parton distributions evaluated at  $Q = 10$  TeV for case (C):  $xu(x)$  (solid line),  $x\bar{u}(x)$  (dashed line), and  $x\tilde{u}(x)$  (dotted line).

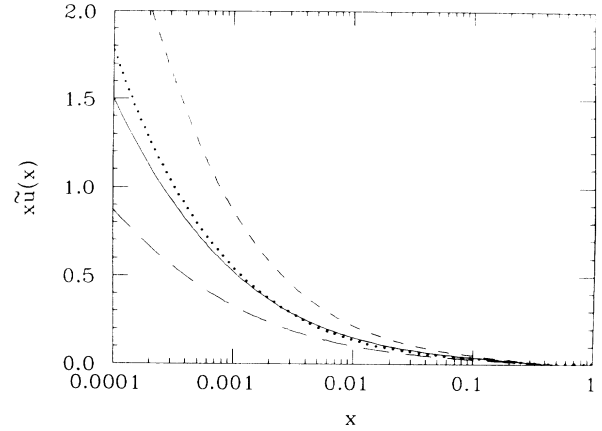


FIG. 6.  $x\bar{u}(x)$  for several combinations of cases and  $Q$  values: case (C),  $Q = 1$  TeV (solid line); case (C),  $Q = 10$  TeV (short dashes); case (D),  $Q = 10$  TeV (dotted line); and case (C),  $Q = 0.3$  TeV (long dashes).

is defined as

$$x\bar{u}(x) \equiv x\bar{u}_L + x\bar{u}_R . \quad (5.1)$$

It is seen that the up-quark distribution is larger than the up-scalar-quark distribution throughout the entire  $x$  range, the difference ranging from a factor of  $\approx 2$  at small  $x$  to a factor of  $\approx 10$  or more for  $x > 0.1$ . The up-antiquark distribution is larger than the up-scalar-quark distribution for  $x \lesssim 0.1$ , but the reverse is true for  $x \gtrsim 0.1$ . The latter is due to the harder  $\bar{u}_v$  valence distribution which is “fed” at larger values of  $x$  by the hard valence  $u_v$  distribution.

Some effects of varying assumptions are shown in Fig. 6, where the  $x\bar{u}$  distribution has been plotted for case (C) with  $Q = 0.3, 1,$  and  $10$  TeV, and for heavy-gluino, heavy-scalar-quark case (D) with  $Q = 10$  TeV. As expected, smaller scalar-quark distributions are produced for lower  $Q$  values but, due to the slow evolution, the differences are factors of 2 rather than orders of magnitude. Changing from case (C) to case (D) at fixed  $Q = 10$

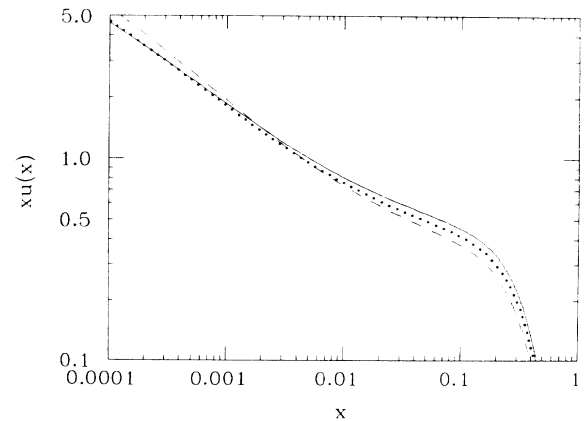


FIG. 7.  $xu(x)$  evaluated at  $Q = 10$  TeV for cases (C) (dashed line), (D) (dotted line), and (F) (solid line).

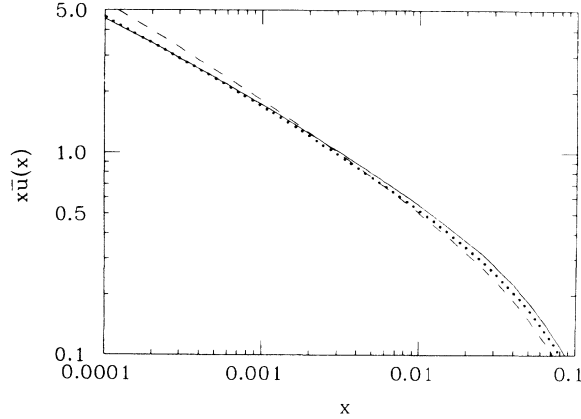


FIG. 8.  $x\bar{u}(x)$  evaluated at  $Q = 10$  TeV for cases (C) (dashed line), (D) (dotted line), and (F) (solid line).

TeV has roughly the same effect on the scalar-quark distribution as reducing  $Q = 10$  TeV to 1 TeV while remaining in case (C).

Two main reasons can be identified for the slowness of growth of the scalar-quark distributions. First, as is well-known, the parton evolution in (S)QCD is only logarithmic. Second, the requirement that  $\alpha_s$  be continuous at the evolution boundaries results, through Eq. (2.10), in a greatly reduced value of  $\Lambda_f$  in regions where the supersymmetric particles are coupled in. This, in turn, reduces the values of  $s$  [see Eq. (2.8)] which control the amount of parton evolution through Eq. (A2) or (A6). Thus, the parton evolution is less than it would have been had  $\Lambda_f$  been fixed. The small  $\Lambda_i/Q_0$  factor in Eq. (2.10) is very effective at reducing  $\Lambda_f$  when matching at large  $Q_0$ . For example, in the final, fully supersymmetric evolution region of case (C), where all the mass thresholds have been passed,  $\Lambda_f$  is reduced from its starting value of 0.2 GeV at  $Q = 2$  GeV to  $\Lambda_f = 4 \times 10^{-5}$  GeV; the corresponding value for case (D) is  $\Lambda_f = 2 \times 10^{-6}$  GeV. For  $Q_{\text{final}} = 10$  TeV, these changes have the effect of reducing  $s$  by about a factor of 2, relative to  $s(\Lambda_f = 0.2 \text{ GeV})$ , in the last evolution region for these cases.

As another measure of the slowness of the evolution, we list in Table I some sample values of the parton momentum fractions, computed by numerical integration of the parton distributions, together with their expected asymptotic values.<sup>15,38</sup> One sees that the scalar-quark momentum fraction grows to at most half of its asymptotic value.

The faster evolution of quark distributions when super-

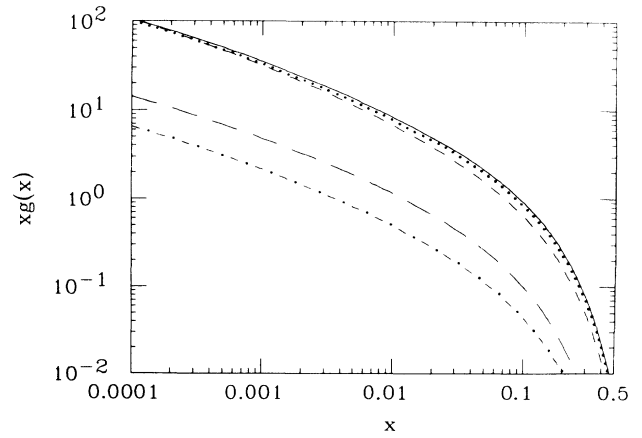


FIG. 9. Gluon ( $g$ ) distributions and gluino ( $\bar{g}$ ) distributions evaluated at  $Q = 1$  TeV for various cases:  $g$ , (F) (solid line);  $g$ , (D) (dotted line);  $g$ , (C) (short dashes);  $\bar{g}$ , (C) (long dashes); and  $\bar{g}$ , (D) (dot-dashed line).

symmetric particles are coupled in can be seen in Fig. 7, which compares the up-quark distribution evaluated at  $Q = 10$  TeV for cases (C), (D), and nonsupersymmetric case (F). For the light-scalar-quark, light-gluino case (C),  $xu(x)$  is somewhat smaller than the others for  $x \gtrsim 0.001$  but is somewhat larger for  $x < 0.001$ ; this sort of behavior is typical of increased scaling violations in QCD. The heavy-scalar-quark, heavy-gluino case (D) interpolates between the other two cases at large  $x$ , but is much closer to case (F) at small  $x$  [it exceeds case (F) by a tiny amount at  $x \approx 10^{-4}$ ]. Physically, when scalar-quarks and gluinos are coupled into the evolution, there are more ways that a quark can split in two and then perhaps be regenerated with a degraded momentum.

In Fig. 8, up-antiquark distributions are plotted under the same assumptions as for Fig. 7. Similar comments to those made about Fig. 7 apply here as well.

Finally, because of the importance of the gluon distribution to Superconducting Super Collider (SSC) physics,<sup>4</sup> we show in Fig. 9 gluon and gluino distributions evaluated at  $Q = 1$  TeV for cases (C), (D) and (F). As expected, when the scalar quarks and gluinos are coupled into the evolution, the gluon distribution is depleted somewhat and a gluino distribution is generated. These effects are more pronounced in the light-scalar-quark, light-gluino case (C) than in the heavy-scalar-quark, heavy-gluino case (D). The gluino distributions are roughly an order of magnitude smaller than the gluon distributions.

TABLE I. Computed momentum fractions and expected asymptotic ( $Q \rightarrow \infty$ ) values for supersymmetric and ordinary cases. The columns do not all add up to 1 due to small computational and rounding errors.

Distribution	Case and $Q$ value (TeV)						SUSY asymptotic	Ordinary asymptotic
	(C), 0.3	(C), 1	(D), 1	(C), 10	(D), 10	(F), 10		
Quark	0.46	0.45	0.48	0.44	0.46	0.50	0.36	0.53
Gluon	0.42	0.39	0.45	0.36	0.40	0.49	0.32	0.47
Scalar quark	0.06	0.08	0.04	0.12	0.08	0.0	0.24	0.0
Gluino	0.06	0.06	0.03	0.07	0.05	0.0	0.08	0.0

TABLE II. Cross sections to produce ordinary  $W$  and  $Z$  in nb. As always, results are only for the decay final state containing an  $e^\pm$ .

Vector boson, case	Initial state, $\sqrt{s}$ (TeV)			
	$p\bar{p}$ , 0.54	$p\bar{p}$ , 2	$pp$ , 40	$p\bar{p}$ , 40
$W^+ + W^-$ , (F)	0.37	1.6	20 <sup>a</sup>	20
$W^+ + W^-$ , (C)	0.28	1.3	17 <sup>a</sup>	17
$Z^0$ , (F)	0.037	0.18	2.4	2.5
$Z^0$ , (C)	0.027	0.14	2.0	2.0

<sup>a</sup> $W^+$  production is 54% of the total.

### B. Cross sections: $\sigma$ and $d\sigma/dy$

Cross sections are computed by summing over all “valence” and “sea” quark and scalar-quark contributions. By convention, all results for cross sections in this paper are for the final state containing an electron (and/or positron). Thus, they implicitly include a factor of the branching ratio  $\Gamma(W \rightarrow e\nu)/\Gamma_W$  or  $\Gamma(Z \rightarrow e^+e^-)/\Gamma_Z$ , except that for  $d^2\sigma/dp_T dy_e$  no simple overall factor of the branching ratio appears since the pole approximation is not used there. These branching ratios are between 5–10% for  $W$ 's and 2–4% for  $Z$ 's.

Table II shows production cross sections for ordinary  $W$  and  $Z$  at CERN SPS, Fermilab Tevatron, and SSC energies for cases (C) and (F). By “ $W^+ + W^-$ ” we mean  $\sigma(h_1 h_2 \rightarrow W^+) + \sigma(h_1 h_2 \rightarrow W^-)$ . The  $\sqrt{s} = 0.54$  TeV results are in reasonable agreement with the CERN data,<sup>43,44</sup> especially considering that  $O(\alpha_s)$  QCD effects have been neglected. However, the supersymmetric results in particular are a bit low and might be ruled out by more precise experimental data, even allowing for  $O(\alpha_s)$  corrections.

Results for production of a 300-GeV vector boson at Tevatron or SSC energies are shown in Table III for cases (C), (E) and (F). Table IV gives cross sections for producing superheavy 1–10-TeV vector bosons at a  $\sqrt{s} = 40$  TeV collider for nonsupersymmetric case (F). The ratios of the  $\sqrt{s} = 40$  TeV results for some sample supersymmetric (SUSY) cases and  $M_B$  values to those for case (F) are plotted in Figs. 10–13.

The cross sections of Tables II–IV and Figs. 10–13 for the SUSY cases are uniformly lower than those for the nonsupersymmetric case (F). One reason for this is the increased total decay width of the vector bosons when supersymmetric decay channels are open, which leads to a

TABLE III. Cross sections to produce a 300-GeV vector boson in pb.

Vector boson, case	Initial state, $\sqrt{s}$ (TeV)		
	$p\bar{p}$ , 2	$pp$ , 40	$p\bar{p}$ , 40
$W^+ + W^-$ , (F)	21.5	634 <sup>a</sup>	647
$W^+ + W^-$ , (E)	13.5	405 <sup>a</sup>	414
$W^+ + W^-$ , (C)	12.1	408 <sup>a</sup>	417
$Z^0$ , (F)	3.5	104	106
$Z^0$ , (E)	2.2	66.3	67.9
$Z^0$ , (C)	2.0	66.8	68.3

<sup>a</sup> $W^+$  production is 55% of the total.

decreased branching ratio into the final state containing an electron (or positron). If scalar quarks are light enough to produce vector bosons by scalar-quark–anti-scalar-quark annihilation, then they are also light enough to be decay products of the produced vector bosons. These increased decay widths alone reduce the cross section by factors of 0.82, 0.79, 0.67, or 0.67 in the ordinary  $W$ , ordinary  $Z$ , heavy  $W$ , or heavy  $Z$  cases, respectively.

As is clear from Figs. 10–13, however, this decay width increase does not account for the entire reduction in  $\sigma$  for the supersymmetry (SUSY) cases. The other important effect is the faster evolution of quark distributions when scalar quarks and gluinos are present, examples of which were shown in Figs. 7 and 8. Reduction of the distributions in the “large”  $x$  region reduces the cross sections that probe this region. The effect is magnified since the formula for the cross section contains two parton distribution factors, one for each incoming hadron. For fixed  $M_B$ , this faster evolution can occur over a larger interval in  $Q^2$ , and thus have a greater effect on  $\sigma$ , for smaller  $M_q, M_g$ . This is why, in Figs. 10–13 for  $M_B = 1–10$  TeV, the light-scalar-quark, light-gluino case (C) determines the bottom and the heavy-scalar-quark, heavy-gluino case (D) determines the top of an “envelope” that encloses the results for cases (A), (B), and (E). For a fixed case in Figs. 10–13,  $\sigma(\text{SUSY})/\sigma(\text{no SUSY})$  decreases with increasing  $M_B$ , again because the evolution interval becomes larger. After removing the effect of the increased SUSY decay width, the largest percentage reduction observed for  $\sigma(\text{SUSY})$  relative to  $\sigma(\text{no SUSY})$  is 45%.

The major source of uncertainty in the amount that  $\sigma$  is reduced due to altered quark distributions is probably

TABLE IV. Cross sections to produce superheavy vector bosons at  $\sqrt{s} = 40$  TeV for nonsupersymmetric case (F) in pb.

Vector boson, initial state	Vector-boson mass (TeV)			
	1	2	5	10
$W^+ + W^-$ , $pp$ <sup>a</sup>	16.5	1.51	0.033	$5.1 \times 10^{-4}$
$W^+ + W^-$ , $p\bar{p}$	18.5	2.03	0.083	$3.6 \times 10^{-3}$
$Z^0$ , $pp$	2.66	0.240	0.0051	$7.7 \times 10^{-5}$
$Z^0$ , $p\bar{p}$	3.00	0.327	0.013	$6.5 \times 10^{-4}$

<sup>a</sup> $W^+$  production is 57%, 59%, 65%, or 72% of the total for  $M_B = 1, 2, 5,$  or  $10$  TeV, respectively.

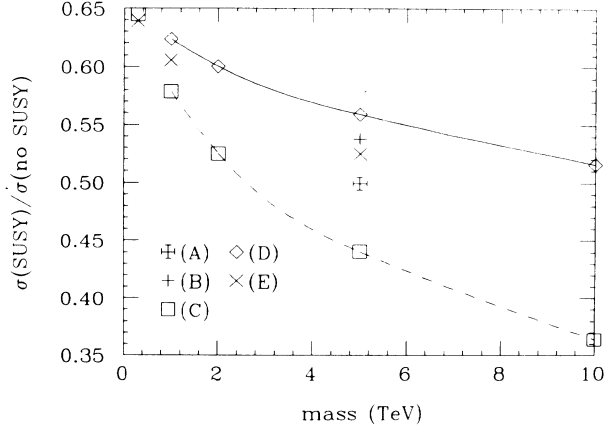


FIG. 10. Ratios of cross sections for various supersymmetric cases to cross sections for nonsupersymmetric case (F), for  $pp \rightarrow W^+ + W^-$  at  $\sqrt{s} = 40$  TeV and for various vector-boson masses. Individual data points are plotted; the solid and dashed lines are only to guide the eye.  $W^+$  production is the same percentage of the total for all cases as it is in Tables III and IV. As always, results are for the decay final state containing an  $e^\pm$ .

in the choice of  $k$ , which determines the values of  $Q = kM_{\tilde{q}}, kM_{\tilde{g}}$  at which the scalar quarks and gluinos are coupled to the evolution. In this paper we use  $k=2$ ; the uncertainty due to varying  $k$  between 1 and 4 can be estimated by comparing the case (D) and case (E) results in Figs. 10–13, since case (E) [(D)] with  $k=2$  can be thought of as case (D) [(E)] with  $k=1$  [4]. The uncertainty in the amount that  $\sigma$  is reduced due to altered quark distributions is thus estimated to be  $\approx 35\%$  for  $M_B = 1$  TeV, and  $\approx 25\%$  for  $M_B = 5$  TeV. Greater sensitivity to the choice of  $k$  is to be expected for smaller  $M_B$  and/or larger SUSY-particle masses.

An apparent exception to our analysis is seen in Table III and Figs. 10–13, which show  $\sigma[\text{case (C)}] \gtrsim \sigma[\text{case (E)}]$  for  $M_B = 300$  GeV at  $\sqrt{s} = 40$  TeV. However, the kin-

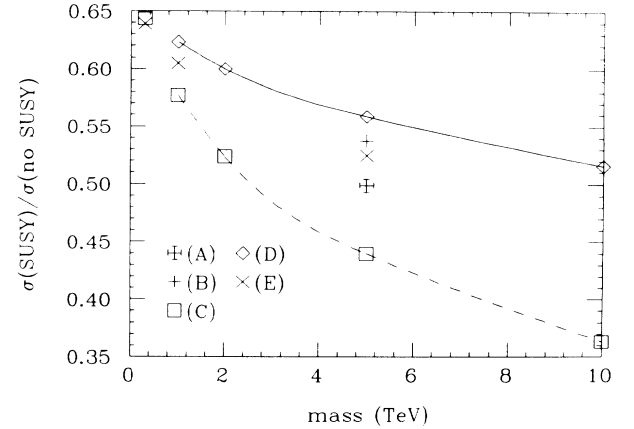


FIG. 12. Same as in Fig. 10 except that cross-section ratios are plotted for  $pp \rightarrow Z^0$ .

matics of this particular process probes very small  $x$  values, where the faster evolving quark distributions in the SUSY cases are relatively equal to or even somewhat larger than those in the non-SUSY case. For example, from Eqs. (3.4) and (3.5) at  $y=0$ ,  $x_1=x_2 = M_B/\sqrt{s} = 7.5 \times 10^{-3}$ , and for  $y \neq 0$  either  $x_1$  or  $x_2$  is always less than this. The greater SUSY decay width accounts here for most of the decrease in  $\sigma(\text{SUSY})$  relative to  $\sigma(\text{no SUSY})$ . One sees in Table III that  $\sigma[\text{case (E)}] > \sigma[\text{case (C)}]$  for  $\sqrt{s} = 2$  TeV since the  $x$  values probed there are no longer so small.

The scalar-quark–anti-scalar-quark annihilation contribution, which increases  $\sigma(\text{SUSY})$  relative to  $\sigma(\text{no SUSY})$ , is quite small (to be quantified in the next subsection) relative to quark-antiquark annihilation and has little noticeable effect on  $\sigma$  (much less than the previous two effects). The smallness of the generated scalar-quark distribution has already been shown in Figs. 5 and 6 and Table I; the effect on  $\sigma$  is smaller yet since factors of both the scalar-quark distribution and the anti-scalar-quark distribution appear there. The main noticeable effect of the scalar-

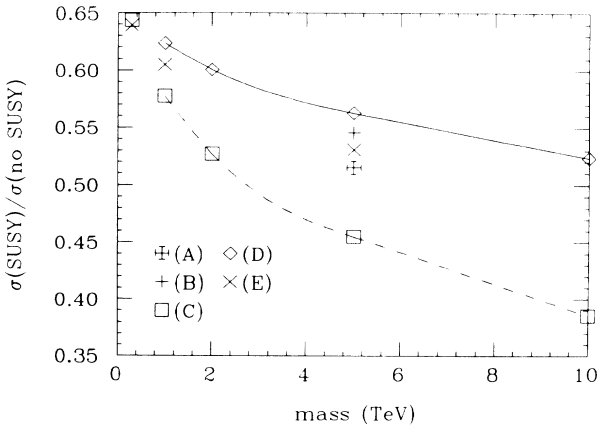


FIG. 11. Same as in Fig. 10 except that cross-section ratios are plotted for  $p\bar{p} \rightarrow W^+ + W^-$ .

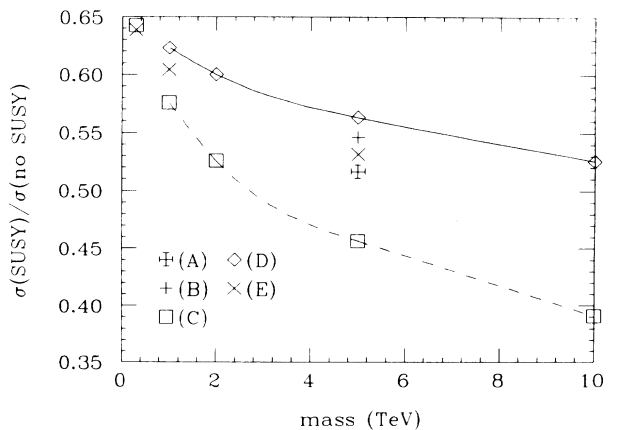


FIG. 13. Same as in Fig. 10 except that cross-section ratios are plotted for  $p\bar{p} \rightarrow Z^0$ .

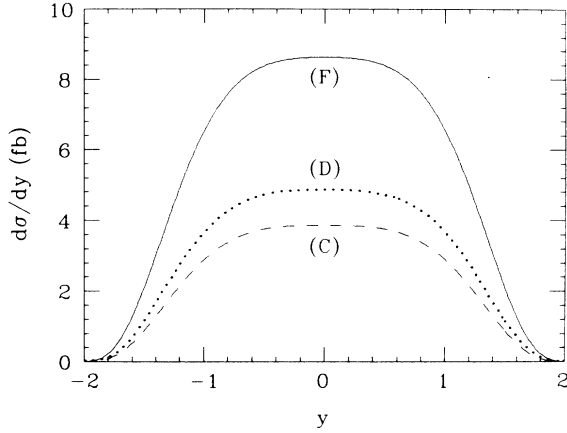


FIG. 14. Rapidity distributions  $d\sigma/dy$  vs vector-boson rapidity  $y$  for  $pp \rightarrow W^+$  with  $\sqrt{s} = 40$  TeV and  $M_B = 5$  TeV. Cases (C) (dashed line), (D) (dotted line), and (F) (solid line) are plotted.

quark contribution in Figs. 10–13 and Table III is that it causes  $\sigma$ [case (C)] to be slightly larger than  $\sigma$ [case (E)] for  $M_B = 300$  GeV and  $\sqrt{s} = 40$  TeV; and in Table II that, for  $\sqrt{s} = 40$  TeV, it causes  $\sigma$ [case (C)] to be slightly larger than the expectation based on the increased supersymmetric decay width.

It could be asked why the reduction in  $\sigma$ , from the terms with two factors of reduced quark distributions, is much larger in magnitude than the increase in  $\sigma$  from the terms with two factors of increased scalar-quark distributions, if the distribution changes are of the same order of magnitude. One simple reason is that, for small  $\delta$ ,  $(1-\delta)^2 = 1 - O(\delta)$  while  $(\delta^2) = O(\delta^2)$ , and  $\delta \gg \delta^2$ . Another reason is that the reduction in quark distributions occurs at moderately large values of  $x$  which are probed for reasonably large values of  $M_B/\sqrt{s}$ , whereas, like any distributions generated by evolution, the scalar-quark distributions are skewed toward smaller  $x$ .

Figures 14–18 show some sample rapidity distribu-

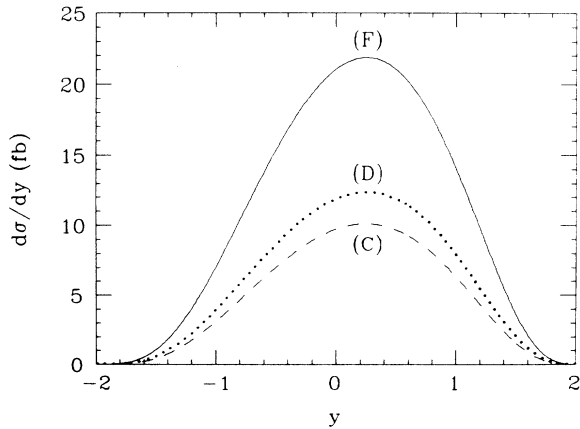


FIG. 15. Same as in Fig. 14 except that the distributions are for  $p\bar{p} \rightarrow W^+$ .

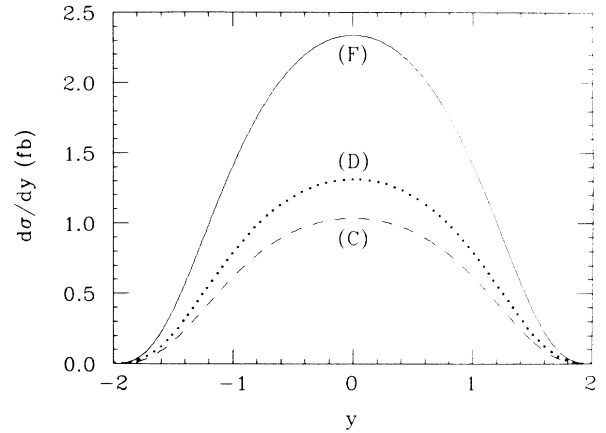


FIG. 16. Same as in Fig. 14 except that the distributions are for  $pp \rightarrow Z^0$ .

tions: supersymmetric and nonsupersymmetric cases are compared for  $W^+$  and  $Z^0$  production at  $\sqrt{s} = 40$  TeV for  $M_B = 5$  and 0.3 TeV. It is seen in all these figures that although the overall normalizations are smaller in the SUSY cases, the shapes of the SUSY distributions are not noticeably different from those of the non-SUSY ones. It was checked that when the curves of SUSY case (C) are rescaled by an overall constant so that they enclose the same areas as the case (F) curves enclose, the two sets of curves become essentially identical, differing only in that the case (C) curves are very slightly ( $\sim 1\%$ ) more peaked at central values of the rapidity.

### C. Angular distributions and asymmetries

The rapidity-integrated  $e^-$  (or  $e^+$  for  $W^+$  production) angular distribution in the vector-boson rest frame can be written as

$$\frac{d\sigma}{d\cos\theta} = a_1(1 + \cos\theta)^2 + a_2(1 - \cos\theta)^2 + a_3(2\sin^2\theta), \quad (5.2)$$

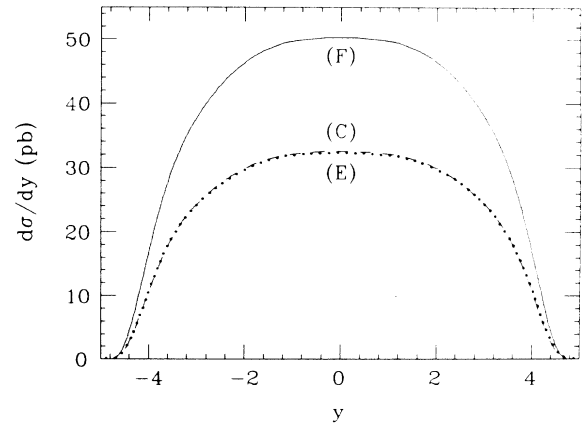


FIG. 17. Same as in Fig. 14 except that the distributions are for  $pp \rightarrow W^+$  with  $M_B = 0.3$  TeV and that here the dotted line is for case (E).

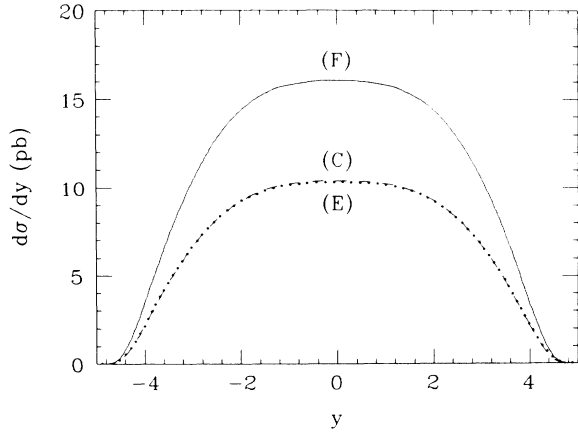


FIG. 18. Same as in Fig. 14 except that the distributions are for  $pp \rightarrow Z^0$  with  $M_B = 0.3$  TeV and that here the dotted line is for case (E).

where the  $a_i$  are normalized such that the angular functions they multiply have equal integrals over  $d \cos \theta$ .  $a_3$  receives contributions from scalar-quark-anti-scalar-quark annihilation only and so is a measure of it. The following relations are found to hold:

$$a_1 = a_2 \quad \text{for } pp \rightarrow W^\pm, Z^0, \quad (5.3)$$

$$a_1(a_2) \quad \text{for } p\bar{p} \rightarrow W^+ = a_2(a_1) \quad \text{for } p\bar{p} \rightarrow W^-, \quad (5.4)$$

$$a_3 \quad \text{for } p\bar{p} \rightarrow W^+ = a_3 \quad \text{for } p\bar{p} \rightarrow W^-. \quad (5.5)$$

For  $p\bar{p} \rightarrow W^-$ ,  $a_1 > a_2$  (and generally  $a_1 \gg a_2$ ) due to the valence-quark contribution.

Directing our attention to the two extreme cases (C) and (F), in Table V we show  $a_3/a_1$  for  $pp \rightarrow W^+$  and for  $(pp \text{ or } p\bar{p}) \rightarrow W^-, Z^0$  for case (C) and several values of  $\sqrt{s}$  and  $M_B$ , while Table VI shows  $a_2/a_1$  for  $p\bar{p} \rightarrow W^-, Z^0$  and cases (C) and (F) [for  $pp$  initial states see Eq. (5.3)]. The  $a_3$  values are uniformly very small and at most a few percent of  $a_1$ , and therefore will be extremely difficult to detect experimentally. This difficulty is made worse by the comparison between Tables V and VI, which shows that  $a_2 \gg a_3$  in most cases so that the  $a_2$  contribution is normally a much larger perturbation of the dominant term in the angular distribution than is the  $a_3$  contribution. Table VI as well shows little difference between the

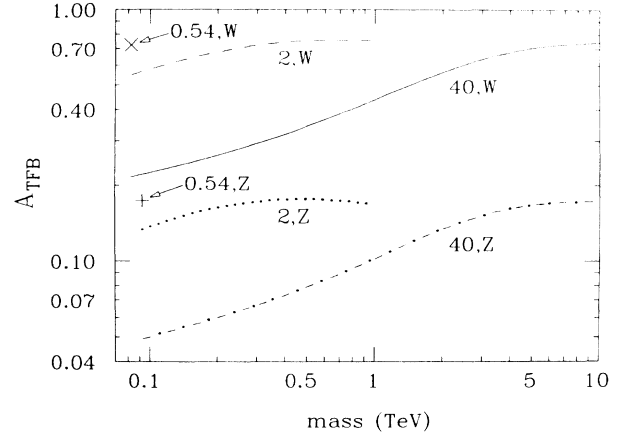


FIG. 19. Total forward-backward asymmetries  $A_{\text{TFB}}$  vs vector-boson mass for  $p\bar{p} \rightarrow W^-$  or  $Z^0$  and case (C). The plotted points and curves are labeled by  $\sqrt{s}$  (in TeV) and vector-boson type.

results for the SUSY and non-SUSY cases. It is interesting to note from Table VI that the  $(1 + \cos \theta)^2$  distribution, characteristic of valence-quark-antiquark annihilation for  $p\bar{p} \rightarrow$  ordinary  $W^-$  and seen at CERN SPS energies,<sup>43</sup> will be significantly altered at SSC energies by the large  $a_2$  contribution due to the sea quarks relevant at the very small  $x$  values probed there. A strategy for experimentally determining the coefficients of the different terms in the angular distributions is suggested in Appendix B, but should be of limited usefulness in finding a scalar-quark contribution due to its expected tiny size.

From Eq. (5.2), the total forward-backward asymmetry, defined in Eq. (3.9), is

$$A_{\text{TFB}} = \frac{3(a_1 - a_2)}{4(a_1 + a_2 + a_3)}. \quad (5.6)$$

From Eqs. (5.3)–(5.5),  $A_{\text{TFB}}(W^\pm, Z^0) = 0$  for  $pp$  initial states, and  $A_{\text{TFB}}(W^+) = -A_{\text{TFB}}(W^-)$ . For  $p\bar{p}$  initial states,  $|A_{\text{TFB}}|$  decreases with increasing  $a_3$  since the scalar-quark contribution is symmetric between the forward and backward hemispheres. However, the pure valence-quark expectation of  $|A_{\text{TFB}}| = \frac{3}{4}$  for  $p\bar{p} \rightarrow W^\pm$  is reduced anyway by the sea-quark contribution.

Sample values of  $A_{\text{TFB}}$  can be computed from Tables V

TABLE V. Values of  $100(a_3/a_1)$  for light-scalar-quark, light-gluino case (C), where the  $a_i$  are defined by Eq. (5.2).

$\sqrt{s}$ (TeV)	$M_B$ (TeV)	$pp \rightarrow W^+$	$pp \rightarrow W^-$	$p\bar{p} \rightarrow W^-$	$pp \rightarrow Z^0$	$p\bar{p} \rightarrow Z^0$
40	Ordinary $W, Z$	1.1	1.2	0.9	1.6	1.5
40	0.3	3.5	3.9	2.6	3.7	3.3
40	1	3.5	4.0	2.1	3.7	3.0
40	5	1.6	1.7	0.6	1.6	0.9
40	10	0.8	0.8	0.3	0.8	0.5
2	Ordinary $W, Z$	0.2	0.2	0.1	0.3	0.2
2	0.3	0.4	0.4	0.1	0.4	0.2
0.54	Ordinary $W, Z$	0.06	0.06	0.02	0.07	0.03

TABLE VI. Values of  $100(a_2/a_1)$ , where  $a_i$  are defined by Eq. (5.2).

$\sqrt{s}$ (TeV)	$M_B$ (TeV)	Case (C)		Case (F)	
		$p\bar{p} \rightarrow W^-$	$p\bar{p} \rightarrow Z^0$	$p\bar{p} \rightarrow W^-$	$p\bar{p} \rightarrow Z^0$
40	Ordinary $W, Z$	55	88	55	88
40	0.3	43	83	43	83
40	1	25	75	26	76
40	5	2.7	63	2.9	63
40	10	0.3	63	0.3	63
2	Ordinary $W, Z$	15	70	15	70
2	0.3	1.8	63	1.9	63
0.54	Ordinary $W, Z$	1.8	63	1.8	63

and VI.  $A_{\text{TFB}}$  is plotted versus  $M_B$  in Fig. 19 for  $p\bar{p} \rightarrow W^-, Z^0$  and various values of  $\sqrt{s}$ . It is clear from the tables that  $A_{\text{TFB}}$  for the SUSY cases differs from  $A_{\text{TFB}}$  for the non-SUSY cases by at most a couple of percent, so only case (C) has been plotted in Fig. 19. In general, larger values of the asymmetry occur for larger values of  $M_B/\sqrt{s}$ , i.e., for larger probed values of  $x$ . When  $M_B/\sqrt{s}$  is sufficiently large, valence-quark-antiquark annihilation completely dominates and an ‘‘asymptotic’’ value of the asymmetry is approached.

As could be expected from the preceding discussion, the rapidity-dependent asymmetry  $A_{\text{FB}}(y)$  of Eq. (3.8) is very similar for the SUSY cases as for the non-SUSY cases. The at most  $\sim$  few percent reductions observed in  $|A_{\text{FB}}(y)|$  for the SUSY cases relative to the non-SUSY cases, consistent with Table V, do not warrant plotting any of these  $A_{\text{FB}}(y)$  vs  $y$  curves here.

#### D. Lepton transverse-momentum distributions

Electron or positron transverse-momentum distributions at  $y_e=0$  from  $W$  production, calculated using Eqs. (3.10) and (3.15), are plotted in Figs. 20–23 for  $pp$  or  $p\bar{p}$  and for various  $M_W$ ,  $\sqrt{s}$ , and SUSY and non-SUSY

cases.  $W^+ + W^-$  means that the  $e^+$  and  $e^-$  distributions have been added together. The deviations of the case (C) curves from the case (F) curves are, as usual, a measure of the maximum effects expected due to supersymmetry. In all the plots, the SUSY curves have shapes similar to those of the non-SUSY curves but are lower by factors  $\sim 2$ . The Jacobian peak at  $p_T \approx M_B/2$  is clearly visible in all the curves. The heavier-scalar-quark and -gluino case curves are closer to the non-SUSY curves but are still somewhat lower, particularly for  $p_T \lesssim M_B/2$ .

In Fig. 24 the Jacobian peak region has been plotted for  $p\bar{p} \rightarrow W^+$ ,  $\sqrt{s}=40$  TeV, and  $M_W=5$  TeV for all the SUSY cases (A)–(E), and for non-SUSY case (F) rescaled by an overall factor of  $\frac{1}{2}$ . It is apparent that the case (F) curve is in fact somewhat more strongly peaked than the SUSY curves, an effect which could be expected from  $\Gamma_W(\text{non-SUSY}) < \Gamma_W(\text{SUSY})$ . Also, the SUSY curves have a common peak  $p_T$ -value which is slightly lower than that for the non-SUSY curve. These are found to be  $2445 \pm 2.5$  GeV and  $2467.5 \pm 2.5$  GeV for the SUSY and non-SUSY curves, respectively. This difference is probably due as well to the difference in  $\Gamma_W$ . Similar small differences in the curve shapes are found for  $pp \rightarrow W^-$  at the same  $\sqrt{s}$  and  $M_W$  (not shown).

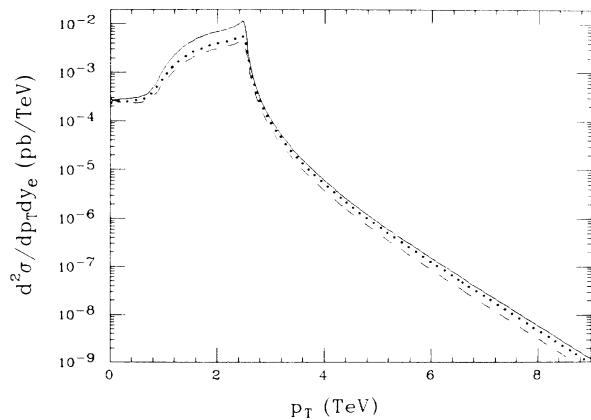


FIG. 20.  $e^+$  transverse-momentum distributions evaluated at  $e^+$  rapidity  $y_e=0$  for  $pp \rightarrow W^+$  with  $\sqrt{s}=40$  TeV and  $M_W=5$  TeV. Cases (C) (dashed line), (D) (dotted line), and (F) (solid line) are plotted.

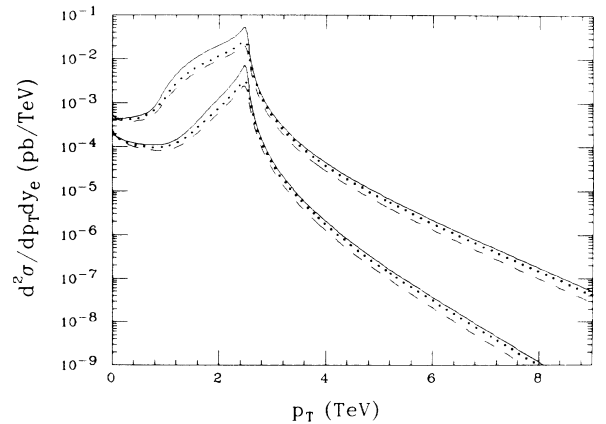


FIG. 21.  $e^\pm$  transverse-momentum distributions evaluated at  $e^\pm$  rapidity  $y_e=0$ . The upper three curves are for  $p\bar{p} \rightarrow W^+ + W^-$ , and the lower three curves are for  $pp \rightarrow W^-$ ; all curves are for  $\sqrt{s}=40$  TeV and  $M_W=5$  TeV. Cases (C) (dashed lines), (D) (dotted lines), and (F) (solid lines) are plotted.

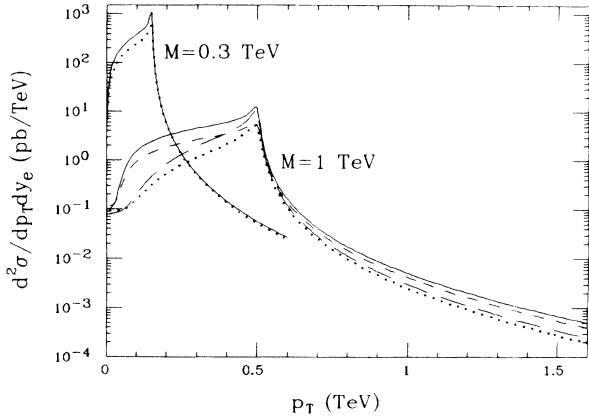


FIG. 22.  $e^\pm$  transverse-momentum distributions at  $y_e=0$ . The two sets of curves are labeled by  $M_W$ ; all curves are for  $\sqrt{s}=40$  TeV. The following reactions and cases are plotted: (i)  $M=0.3$  TeV set:  $pp \rightarrow W^+$ , (F) (solid line) and  $pp \rightarrow W^+$ , (C) (dotted line); (ii)  $M=1$  TeV set:  $pp \rightarrow W^+$ , (F) (solid line);  $pp \rightarrow W^+$ , (C) (short dashes);  $pp \rightarrow W^-$ , (F) (long dashes); and  $pp \rightarrow W^-$ , (C) (dotted line).

The differences in the magnitudes of the case (A)–(E) curves in Fig. 24 are reasonable considering the different scalar-quark and gluino mass assumptions they represent, and agree with the pattern observed in Fig. 10 for the total cross sections, i.e., smaller scalar quark and gluino masses result in smaller cross sections. As  $\Gamma_W$  is the same for each of these curves (A)–(E), these differences must be attributed to the differences in the evolution of the quark distributions. However, the curve shapes are essentially the same for each case. In all of Figs. 20–24, the scalar-quark–anti-scalar-quark annihilation contribution is small compared to the quark-antiquark annihilation contribution for all values of  $p_T$ , so that no direct signature for the scalar-quark–anti-scalar-quark contribution can be identified.

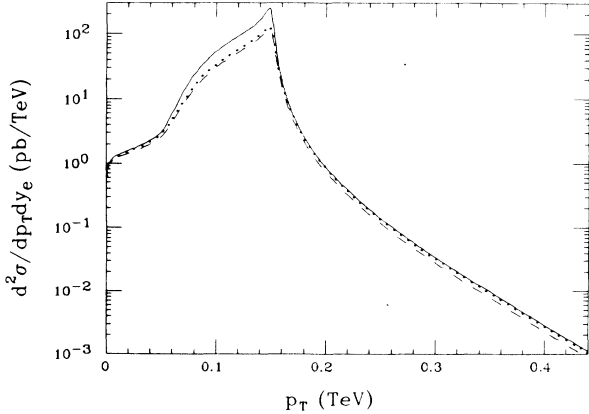


FIG. 23.  $e^\pm$  transverse-momentum distributions at  $y_e=0$  for  $p\bar{p} \rightarrow W^+ + W^-$  with  $\sqrt{s}=2$  TeV and  $M_W=0.3$  TeV. Cases (C) (dashed line), (E) (dotted line), and (F) (solid line) are plotted.

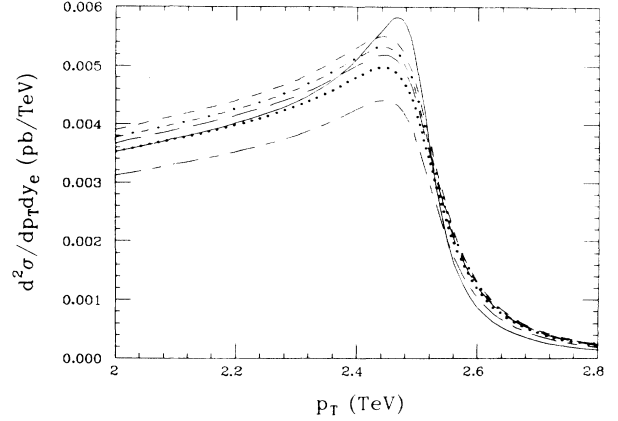


FIG. 24.  $e^+$  transverse-momentum distribution at  $y_e=0$  for  $pp \rightarrow W^+$  with  $\sqrt{s}=40$  TeV and  $M_W=5$  TeV, in the vicinity of the Jacobian peak. The following cases are plotted: case (F) rescaled by a factor of  $\frac{1}{2}$  (solid line), (D) (short dashes), (B) (dot-dashed line), (E) (long dashes), (A) (dotted line), and (C) (alternating long and short dashes).

## VI. CONCLUSION

Production in  $pp$  and  $p\bar{p}$  collisions of ordinary and possible new heavy vector bosons decaying to final states containing  $e^\pm$  has been studied in supersymmetric QCD in the leading-logarithm approximation. Parton distributions were computed for both the nonsupersymmetric case and for various supersymmetric scalar-quark and gluino mass scenarios, and detailed comparisons were made between SUSY and non-SUSY cases for various cross sections. Because of the slowness of the evolution of the scalar-quark distributions, the potential direct effects of scalar-quark–anti-scalar-quark annihilation on the total cross sections, angular distributions, asymmetries, and  $e^\pm$  transverse-momentum distributions were found to be small for a range of values of  $\sqrt{s}$ ,  $M_B$ ,  $M_{\tilde{q}}$ , and  $M_{\tilde{g}}$  expected to be accessible in the near future, so no reasonable signature for this contribution could be found. The scalar-quark–anti-scalar-quark annihilation contribution was quantified to be at most a few percent of the quark-antiquark annihilation contribution.

However, the introduction of supersymmetry produced “indirect” effects on the results for two reasons. First, the availability of supersymmetric decay channels increased the vector-boson total decay widths, which in turn reduced the branching ratio into final states containing  $e^\pm$ . Second, the coupling of scalar-quark and gluino degrees of freedom to the Altarelli-Parisi parton evolution caused the quark distributions to evolve faster with increasing  $Q^2$  than if these supersymmetric channels were closed. These two effects combined to produce cross sections smaller by factors of at most 2–3 in the SUSY cases as compared to the non-SUSY case. The shapes of distributions were generally the same in the two cases, except that the  $e^\pm$  transverse-momentum distributions were somewhat less sharply peaked and were peaked at slightly lower- $p_T$  values for the SUSY cases. The only superheavy vector bosons considered were copies of the

standard  $W$  and  $Z$ , and the initial low-energy quark and gluon distributions were fixed, but our conclusions about differences between the SUSY and non-SUSY cases are expected to be valid for more general assumptions as well.

Experimentally, the lowered cross sections in the SUSY cases would make it somewhat more difficult to discover and study new vector bosons at higher-energy hadronic colliders, but not substantially so. For example, assuming an integrated luminosity of  $10^4 \text{ pb}^{-1}$  at a  $\sqrt{s} = 40 \text{ TeV}$   $pp$  collider, for an  $M_W = 5 \text{ TeV}$   $W^\pm$  decaying into  $e^\pm \nu$ , our calculations indicate 330 events without SUSY but only 145 events in SUSY case (C); for  $M_W = 10 \text{ TeV}$ , the corresponding numbers are 5 events and 2 events, respectively. However, attempts to study couplings by measuring forward-backward asymmetries are as reasonable with SUSY as without SUSY, due to the smallness of the scalar-quark-anti-scalar-quark annihilation contribution. Also, the Jacobian peak in the  $e^\pm p_T$  distribution, which is so useful for identifying vector bosons, is clearly visible in either case.

On the other hand, once a new vector boson has been discovered and its couplings determined, one could contemplate discovering supersymmetry or putting lower bounds on SUSY-particle masses using the results of this paper, i.e., if SUSY exists, the production cross sections would be somewhat lower than expected, decay widths would be larger, etc. Such effects could be discernible for supersymmetric masses sufficiently small that decays into SUSY-particles make a reasonable contribution to  $\Gamma_B$ , say for  $M \lesssim M_B/3$ . One would need to fix the magnitude of the couplings by some other method first since, e.g.,  $\Gamma$  and  $\sigma$  both depend on  $g$ . It is perhaps worthwhile even to consider ordinary  $W$  and  $Z$  production in this context. Of course, one would ordinarily expect to discover supersymmetry much more easily (and earlier) by looking for direct production of superpartners.

#### ACKNOWLEDGMENTS

I am grateful to J.F. Owens for helpful discussions. This work was supported in part by the U.S. Department of Energy.

#### APPENDIX A: INTEGRATION OF EVOLUTION EQUATIONS

Any of the Altarelli-Parisi equations used for the evolution of nonsinglet or singlet distributions may be written in the form

$$\frac{d\mathbf{g}(x,s)}{ds} = a_f \underline{P} \otimes \mathbf{g}(x,s), \quad (\text{A1})$$

where  $\mathbf{g}$  is an  $m$ -component column vector of  $x^2$  times parton distributions (with arguments made explicit in this Appendix) and  $\underline{P}$  is an  $m \times m$  matrix of integral kernels. In this paper,  $m$  can be 1, 2, 3, or 4. Given  $\mathbf{g}(x,0)$  as a boundary condition, Eq. (A1) is solved numerically for  $\mathbf{g}(x,s)$  by using an extension of a method that to our knowledge was first suggested in Ref. 34. After integrating Eq. (A1) over  $ds$ , a sequence of approximants  $\mathbf{g}_k(x,s)$  to the solution  $\mathbf{g}(x,s)$  can be defined by iteration to be

$$\mathbf{g}_k(x,s) = \sum_{j=0}^k \frac{(a_f s)^j}{j!} \underline{P}^j \otimes \mathbf{g}(x,0), \quad (\text{A2})$$

where

$$\underline{P}^j \otimes \mathbf{g}(x,0) \equiv \underline{P} \otimes (\underline{P} \otimes \{ \cdots [\underline{P} \otimes \mathbf{g}(x,0)] \cdots \}). \quad (\text{A3})$$

Equation (A2) defines a perturbation series in  $a_f s$  which is easily summed:

$$\begin{aligned} \mathbf{g}(x,s) &= \lim_{k \rightarrow \infty} \mathbf{g}_k(x,s) \\ &= \exp(a_f s \underline{P}) \otimes \mathbf{g}(x,0). \end{aligned} \quad (\text{A4})$$

For a given  $s$ , a mesh of  $x$  points is set up for  $10^{-5} \leq x \leq 1$  and the  $\mathbf{g}_k$ 's are computed for each  $x$ . The convolution integrals are done using cubic spline quadrature.<sup>46</sup> The computation is concluded when  $k$  is reached such that

$$\max_{x \in \text{mesh}; i} \left| \frac{\mathbf{g}_k^i(x,s) - \mathbf{g}_{k-1}^i(x,s)}{\mathbf{g}_k^i(x,s)} \right| \leq 10^{-3}, \quad (\text{A5})$$

where  $i$  labels the  $i$ th component of the vector  $\mathbf{g}$ . The finite number of interpolation points ("knots") in the spline integrations presents an additional source of inaccuracy. This error was reduced to an estimated maximum of  $\approx 20\%$  for  $x \approx 10^{-5}$ ,  $\approx 10\%$  for  $x \approx 10^{-4}$ , and a negligible amount for  $x \gtrsim 5 \times 10^{-4}$ . Errors can compound when evolution occurs over several consecutive regions, however. It should also be noted that non-valence-quark and -scalar-quark distributions are functions of differences between singlet and nonsinglet distributions which can be equal to several decimals for  $x$  close to 1, resulting occasionally in negative parton distributions. In practice this is only a problem for  $x \gtrsim 0.95$  where these distributions are negligibly small anyway, so to avoid tiny negative cross sections as much as possible these signs were flipped to positive, producing parton distributions that are equivalent within the numerical errors.

The evolution algorithm was checked in several ways. In the 4 quarks + gluon case (i), satisfactory agreement was found with the Duke and Owens parametrization<sup>31</sup> and direct numerical results<sup>47</sup> which used a predictor-corrector method,<sup>39</sup> as well as with distributions derived using nonsinglet<sup>39,48</sup> and singlet<sup>49</sup> integral kernels in the method of Gross.<sup>50</sup> Also, good agreement was found in case (i) between the moments of our evolved distributions and the evolved moments of the starting distributions using the usual nonsinglet and diagonalized singlet moments evolution equations.<sup>38</sup>

However, the most useful check for all nine evolution subroutines originates with the observation that Eq. (A4) is merely the  $x$ -space version of the standard evolution formula for moments.<sup>16</sup> That is, by taking the moment of Eq. (A2) and using the standard convolution theorem for Mellin transforms (Ref. 38)  $j$  times for the  $j$ th term in the sum, one obtains

$$\mathbf{g}_k^{(n)}(s) = \sum_{j=0}^k \frac{(a_f s \underline{P}^{(n)})^j}{j!} \mathbf{g}^{(n)}(0), \quad (\text{A6})$$

where

$$f^{(n)} \equiv \int_0^1 dx x^{n-1} f(x). \quad (\text{A7})$$

Now, letting  $k \rightarrow \infty$ , or equivalently taking the moment of Eq. (A4), gives

$$\begin{aligned} \mathbf{g}^{(n)}(s) &= \lim_{k \rightarrow \infty} \mathbf{g}_k^{(n)}(s) \\ &= \exp(a_f s \underline{P}^{(n)}) \mathbf{g}^{(n)}(0) \\ &= \left[ \frac{\ln(Q^2/\Lambda_f^2)}{\ln(Q_0^2/\Lambda_f^2)} \right]^{a_f \underline{P}^{(n)}} \mathbf{g}^{(n)}(0), \end{aligned} \quad (\text{A8})$$

which is precisely the standard formula.<sup>16</sup> After computing the moments of the starting distributions, Eq. (A8) for  $1 \times 1$  evolution or Eq. (A6) for  $2 \times 2$ ,  $3 \times 3$ , or  $4 \times 4$  evolution is used to evolve the moments up to  $Q^2$ . In particular, it is never necessary to diagonalize the  $\underline{P}^{(n)}$ 's. One merely chooses  $k$  large enough in Eq. (A6) for sufficient convergence to have occurred. The resulting moments are then compared to the moment integrals of the distributions evolved using Eq. (A2). Since only simple matrix multiplications are involved in Eqs. (A6) or (A8), this entire check takes a negligible fraction of the total computing time. Agreement in all subroutines was typically better than  $10^{-3}$  relative error for the first 50 moments, except that the agreement of  $n=1$  moments was somewhat worse due to poorer convergence and singular behavior of distributions near  $x=0$ .

It should be noted that one disadvantage of the numerical integration method described here compared to, say, the predictor-corrector method,<sup>39</sup> is that here distributions can be computed for only one value of  $s$ , i.e.,  $Q$ , at a time. This is not a particular disadvantage for purposes of this paper since  $Q$  is fixed to be a particular vector-boson mass of interest. However, computational runs at a number of different  $s$  values would be required in order to obtain a simple parton parametrization valid for a range of  $x$  and  $s$ . In this paper, cross sections are computed directly from the numerical results for parton distributions using cubic splines to interpolate in  $x$ ; no other parametrizations of the parton distributions are made.

## APPENDIX B: ANALYSIS OF ANGULAR DISTRIBUTIONS

In this appendix, a method is suggested to experimentally resolve different contributions to the lepton angular distribution in the produced vector-boson rest frame. Let  $\sigma(\cos\theta)$  represent either  $d\sigma/d\cos\theta$  or  $d^2\sigma/d\cos\theta dy$ . According to Sec. III, in the supersymmetric parton model there is a theoretical prediction

$$\sigma_{\text{th}}(\cos\theta) = \alpha_0(1 + \cos\theta)^2 + \alpha_1(1 - \cos\theta)^2 + \alpha_2(1 - \cos^2\theta). \quad (\text{B1})$$

Choosing a complete set of Legendre polynomials  $P_i(x)$ ,  $i \geq 0$ , taken to be orthonormal on  $-1 \leq x \leq 1$ , where<sup>51</sup>

$$P_0(x) = (\frac{1}{2})^{1/2}, \quad (\text{B2})$$

$$P_1(x) = [(\frac{3}{2})^{1/2}]x, \quad (\text{B3})$$

$$P_2(x) = [(\frac{5}{8})^{1/2}](3x^2 - 1), \quad (\text{B4})$$

the experimentally observed cross section may be written as

$$\sigma_{\text{expt}}(\cos\theta) = \sum_{i=0}^{\infty} \beta'_i P_i(\cos\theta), \quad (\text{B5})$$

where

$$\beta'_i = \int_{-1}^1 d\cos\theta P_i(\cos\theta) \sigma_{\text{expt}}(\cos\theta); \quad (\text{B6})$$

these integrals can be done numerically.

If Eq. (B1) is approximately correct, then  $\beta'_i \approx 0$  for  $i \geq 3$  and we can write a truncated cross section

$$\begin{aligned} \sigma_{\text{expt}}^{\text{tr}}(\cos\theta) &= \sum_{i=0}^2 \beta'_i P_i(\cos\theta) \\ &= \alpha'_0(1 + \cos\theta)^2 + \alpha'_1(1 - \cos\theta)^2 \\ &\quad + \alpha'_2(1 - \cos^2\theta), \end{aligned} \quad (\text{B7})$$

where the  $\alpha'_i$  are related to the  $\beta'_i$  by a simple computation, and the assumption that  $\sigma_{\text{expt}} \approx \sigma_{\text{expt}}^{\text{tr}}$  can be checked. The  $\alpha'_i$  thus derived can be compared with or used to put bounds on theoretically predicted  $\alpha_i$ .

<sup>1</sup>P. Fayet and S. Ferrara, Phys. Rep. **32**, 249 (1977).

<sup>2</sup>H. E. Haber and G. L. Kane, Phys. Rep. **117**, 75 (1985).

<sup>3</sup>S. Dawson, E. Eichten, and C. Quigg, Phys. Rev. D **31**, 1581 (1985).

<sup>4</sup>E. Eichten, I. Hinchliffe, K. Lane, and C. Quigg, Rev. Mod. Phys. **56**, 579 (1984).

<sup>5</sup>J. Ellis, in *Superstrings and Supergravity*, proceedings of the 28th Scottish Universities Summer School in Physics, Edinburgh, 1985, edited by A. T. Davies and D. G. Sutherland (SUSSP, Edinburgh, 1986), p. 399.

<sup>6</sup>G. Arnison *et al.*, Phys. Lett. **139B**, 115 (1984); C. Rubbia, in *Proceedings of the 1985 International Symposium on Lepton and Photon Interactions at High Energies*, Kyoto, Japan, 1985,

edited by M. Konuma and K. Takahashi (Research Institute for Fundamental Physics, Kyoto University, Kyoto, 1986), p. 242; J. Rohlf, in *Proceedings of the Oregon Meeting*, Annual Meeting of the Division of Particles and Fields of the APS, Eugene, Oregon, 1985, edited by R. C. Hwa (World Scientific, Singapore, 1986), p. 66.

<sup>7</sup>R. M. Barnett, H. E. Haber, and G. L. Kane, Nucl. Phys. **B267**, 625 (1986).

<sup>8</sup>J. Ellis, G. Gelmini, C. Jarlskog, G. G. Ross, and J. W. F. Valle, Phys. Lett. **150B**, 142 (1985); G. G. Ross and J. W. F. Valle, *ibid.* **151B**, 375 (1985); S. Dawson, Nucl. Phys. **B261**, 297 (1985).

<sup>9</sup>S. D. Drell and T.-M. Yan, Phys. Rev. Lett. **25**, 316 (1970).

- <sup>10</sup>G. Altarelli, R. K. Ellis, and G. Martinelli, Nucl. Phys. **B157**, 461 (1979).
- <sup>11</sup>L. B. Okun, *Leptons and Quarks* (North-Holland, Amsterdam, 1982).
- <sup>12</sup>G. Altarelli and G. Parisi, Nucl. Phys. **B126**, 298 (1977).
- <sup>13</sup>B. A. Campbell, J. Ellis, and S. Rudaz, Nucl. Phys. **B198**, 1 (1982); I. Antoniadis, C. Kounnas, and R. Lacaze, *ibid.* **B211**, 216 (1983).
- <sup>14</sup>C. Kounnas and D. A. Ross, Nucl. Phys. **B214**, 317 (1983).
- <sup>15</sup>S. K. Jones and C. H. Llewellyn Smith, Nucl. Phys. **B217**, 145 (1983).
- <sup>16</sup>M. J. Herrero, C. Lopez, and F. J. Yndurain, Nucl. Phys. **B244**, 207 (1984).
- <sup>17</sup>H. E. Haber, in *Proceedings of the 1984 Summer Study on the Design and Utilization of the Superconducting Super Collider*, edited by R. Donaldson and J. G. Morfin (American Physical Society, New York, 1984), p. 125.
- <sup>18</sup>G. Arnison *et al.*, Phys. Lett. **122B**, 103 (1983); **126B**, 398 (1983); M. Banner *et al.*, *ibid.* **122B**, 476 (1983); P. Bagnaia *et al.*, *ibid.* **129B**, 130 (1983).
- <sup>19</sup>R. N. Mohapatra, in *Quarks, Leptons, and Beyond*, edited by H. Fritzsch, R. D. Peccei, H. Saller, and F. Wagner (Plenum, New York, 1985), p. 219.
- <sup>20</sup>R. W. Robinett and J. L. Rosner, Phys. Rev. D **25**, 3036 (1982); R. W. Robinett, *ibid.* **26**, 2388 (1982); C. N. Leung and J. L. Rosner, *ibid.* **29**, 2132 (1984).
- <sup>21</sup>E. Farhi and L. Susskind, Phys. Rep. **74**, 277 (1981).
- <sup>22</sup>F. Wilczek and A. Zee, Phys. Rev. Lett. **42**, 421 (1979); D. R. T. Jones, G. L. Kane, and J. Leveille, Nucl. Phys. **B198**, 45 (1982).
- <sup>23</sup>U. Baur, in *Progress in Electroweak Interactions*, proceedings of the 21st Rencontre de Moriond, Les Arcs, France, 1986, edited by J. Tran Thanh Van (Editions Frontières, Gif-sur-Yvette, France, 1986), p. 139.
- <sup>24</sup>S. M. Barr, Phys. Rev. Lett. **55**, 2778 (1985); E. Cohen, J. Ellis, K. Enqvist, and D. V. Nanopoulos, Phys. Lett. **165B**, 76 (1985); V. Barger, N. G. Deshpande, and K. Whisnant, Phys. Rev. Lett. **56**, 30 (1986); L. S. Durkin and P. Langacker, Phys. Lett. **166B**, 436 (1986).
- <sup>25</sup>D. London and J. L. Rosner, Phys. Rev. D **34**, 1530 (1986); V. Barger, N. G. Deshpande, J. L. Rosner, and K. Whisnant, *ibid.* **35**, 2893 (1987).
- <sup>26</sup>E. Witten, Nucl. Phys. **B258**, 75 (1985); J. D. Breit, B. A. Ovrut, and G. C. Segre, Phys. Lett. **158B**, 33 (1985); M. Dine, V. Kaplunovsky, M. Mangano, C. Nappi, and N. Seiberg, Nucl. Phys. **B259**, 549 (1985); P. Binetruy, S. Dawson, I. Hinchliffe, and M. Sher, *ibid.* **B273**, 501 (1986); J. Ellis, K. Enqvist, D. V. Nanopoulos, and F. Zwirner, *ibid.* **B276**, 14 (1986).
- <sup>27</sup>P. Langacker, R. W. Robinett, and J. L. Rosner, Phys. Rev. D **30**, 1470 (1984).
- <sup>28</sup>J. F. Gunion, in *Proceedings of the 1984 Summer Study on the Design and Utilization of the Superconducting Super Collider*, (Ref. 17), p. 147.
- <sup>29</sup>Rubbia and Rohlf (Ref. 6).
- <sup>30</sup>N. G. Deshpande, J. F. Gunion, and H. E. Haber, in *Proceedings of the 1984 Summer Study on the Design and Utilization of the Superconducting Super Collider* (Ref. 17), p. 119.
- <sup>31</sup>D. W. Duke and J. F. Owens, Phys. Rev. D **30**, 49 (1984).
- <sup>32</sup>L. F. Abbott and M. B. Wise, Nucl. Phys. **B176**, 373 (1980).
- <sup>33</sup>T. Appelquist and J. Carazzone, Phys. Rev. D **11**, 2856 (1975); E. Witten, Nucl. Phys. **B104**, 445 (1976).
- <sup>34</sup>V. Barger, S. Jacobs, J. Woodside, and K. Hagiwara, Phys. Rev. D **33**, 57 (1986).
- <sup>35</sup>J.-P. Revol, in *Sixth Workshop on Grand Unification*, edited by S. Rudaz and T. F. Walsh (World Scientific, Singapore, 1986), p. 275.
- <sup>36</sup>V. Barger, K. Hagiwara, W.-Y. Keung, and J. Woodside, Phys. Rev. D **31**, 528 (1985).
- <sup>37</sup>G. Altarelli, R. K. Ellis, M. Greco, and G. Martinelli, Nucl. Phys. **B246**, 12 (1984).
- <sup>38</sup>A. J. Buras, Rev. Mod. Phys. **52**, 199 (1980).
- <sup>39</sup>A. Devoto, D. W. Duke, J. F. Owens, and R. G. Roberts, Phys. Rev. D **27**, 508 (1983).
- <sup>40</sup>B. Kayser and R. E. Shrock, Phys. Lett. **112B**, 137 (1982); B. Kayser, Phys. Rev. D **26**, 1662 (1982).
- <sup>41</sup>R. F. Peierls, T. L. Trueman, and L.-L. Wang, Phys. Rev. D **16**, 1397 (1977); J. Kogut and J. Shigemitsu, Nucl. Phys. **B129**, 461 (1977).
- <sup>42</sup>F. Halzen and D. M. Scott, Phys. Lett. **78B**, 318 (1978); F. Halzen, A. D. Martin, and D. M. Scott, Phys. Rev. D **25**, 754 (1982); G. Altarelli, R. K. Ellis, and G. Martinelli, Z. Phys. C **27**, 617 (1985).
- <sup>43</sup>G. Arnison *et al.*, Phys. Lett. **166B**, 484 (1986).
- <sup>44</sup>J. A. Appel *et al.*, Z. Phys. C **30**, 1 (1986).
- <sup>45</sup>W. J. Marciano, Phys. Rev. D **20**, 274 (1979); M. B. Einhorn and D. R. T. Jones, Nucl. Phys. **B196**, 475 (1982).
- <sup>46</sup>J. H. Ahlberg, E. N. Nilson, and J. L. Walsh, *The Theory of Splines and Their Applications* (Academic, New York, 1967).
- <sup>47</sup>J. F. Owens (private communication).
- <sup>48</sup>K. Kato, Y. Shimizu, and H. Yamamoto, Prog. Theor. Phys. **63**, 1295 (1980).
- <sup>49</sup>K. Kato and Y. Shimizu, Prog. Theor. Phys. **64**, 703 (1980).
- <sup>50</sup>D. J. Gross, Phys. Rev. Lett. **32**, 1071 (1974).
- <sup>51</sup>J. D. Jackson, *Classical Electrodynamics* (Wiley, New York, 1975).